DIGITAL ACCESS TO SCHOLARSHIP AT HARVARD
DASH.HARVARD.EDU

HARVARD LIBRARY
Office for Scholarly Communication

Enriched Basalts at Segment Centers: The Lucky Strike (37°17#N) and Menez Gwen (37°50#N) Segments of the Mid#Atlantic Ridge

Citation
Gale, Allison, Stephane Escrig, Elizabeth J. Gier, Charles H. Langmuir and Steven L. Goldstein. 2011. Enriched basalts at segment centers: The Lucky Strike (37°17#N) and Menez Gwen (37°50#N) segments of the Mid-Atlantic Ridge. Geochemistry Geophysics Geosystems 12(6): Q06016.

Published Version
doi:10.1029/2010GC003446

Permanent link
http://nrs.harvard.edu/urn-3:HUL.InstRepos:9468170

Terms of Use
This article was downloaded from Harvard University's DASH repository, and is made available under the terms and conditions applicable to Other Posted Material, as set forth at http://nrs.harvard.edu/urn-3:HUL.InstRepos:dash.current.terms-of-use#LAA

Share Your Story

The Harvard community has made this article openly available.
Please share how this access benefits you. Submit a story .

Accessibility

Geochemistry Geophysics Geosystems G3

Article
Volume 12, Number 6
25 June 2011
Q06016, doi:10.1029/2010GC003446
ISSN: 1525-2027

Published by AGU and the Geochemical Society

Enriched basalts at segment centers: The Lucky Strike (37°17′N) and Menez Gwen (37°50′N) segments of the Mid-Atlantic Ridge

Allison Gale and Stephane Escrig
Department of Earth and Planetary Sciences, Harvard University, 20 Oxford Street, Cambridge, Massachusetts 02138, USA (agale@fas.harvard.edu)

Elizabeth J. Gier
Department of Geology and Geophysics, SOEST, University of Hawai'i at Mānoa, Honolulu, Hawaii 96822, USA

Charles H. Langmuir
Department of Earth and Planetary Sciences, Harvard University, 20 Oxford Street, Cambridge, Massachusetts 02138, USA

Steven L. Goldstein
Lamont-Doherty Earth Observatory, Department of Earth and Environmental Sciences, Columbia University, 61 Route 9W, Palisades, New York 10964, USA

[1] Basalts from the Mid-Atlantic Ridge change progressively in composition with increasing distance from the Azores platform. Study of the Lucky Strike and Menez Gwen segments reveals much complexity in the gradient. Both segments contain only basalts enriched relative to normal mid-oceanic ridge basalt, but in two distinct groups. Moderately enriched basalts occur throughout the segments, with proximal Menez Gwen enriched relative to Lucky Strike. Highly enriched basalts occur at segment centers. Incompatible element ratios of the highly enriched basalts exceed those of the Azores platform, while isotopic compositions are less enriched. These observations can be explained by a low-degree melt of garnet-bearing Azores mantle added to mantle depleted by previous melt extraction. Melting this "metasomatized" mantle produces lavas that match the enriched samples. The Azores gradient cannot be explained by simple two-component mixing; rather, it reflects recent melt extraction and addition processes related to southward flow of the Azores plume. The Azores gradient also permits tests of segmentation models. Central supply models predict step functions in chemical compositions between segments. Within-segment gradients require vertical supply. Central supply is supported by robust central volcanoes, thicker crust at segment centers, and a step function in isotopes between the segments. The lava diversity at segment centers, however, requires batches of distinct magma that are preserved through melting and melt delivery. Within-segment gradients in moderately incompatible element ratios support a component of multiple supply. The data suggest partial homogenization of magma within a segment and preferential melt focusing to segment centers with some vertical transport.

Components: 15,300 words, 11 figures, 3 tables.

Keywords: Lucky Strike; mid-ocean ridge basalt; partial melting; trace element geochemistry.

Index Terms: 1021 Geochemistry: Composition of the oceanic crust; 1065 Geochemistry: Major and trace element geochemistry; 3035 Marine Geology and Geophysics: Midocean ridge processes.

Received 24 November 2010; **Revised** 9 May 2011; **Accepted** 9 May 2011; **Published** 25 June 2011.

Copyright 2011 by the American Geophysical Union

Gale, A., S. Escrig, E. J. Gier, C. H. Langmuir, and S. L. Goldstein (2011), Enriched basalts at segment centers: The Lucky Strike (37°17′N) and Menez Gwen (37°50′N) segments of the Mid-Atlantic Ridge, *Geochem. Geophys. Geosyst.*, *12*, Q06016, doi:10.1029/2010GC003446.

1. Introduction

[2] Classical work by *Schilling* [1975] established a gradient in ridge depth and chemical compositions of basalts extending southward from the Azores hot spot. Basalts near the hot spot were more enriched in highly incompatible elements and $^{87}Sr/^{86}Sr$ [*White and Schilling*, 1978], and this enrichment lessened southward until depleted mid-oceanic ridge basalts (MORBs) were encountered south of the Hayes fracture zone near 34°N.

[3] As maps of ocean ridges grew more detailed, it became clear that the concept of "gradient" needed refinement. Ocean ridges consist of a series of ridge segments defined by transform faults and other offsets [*Sinton et al.*, 1991]. Segments tend to be shallow in their central regions and deeper at their ends, so the "regional gradient" in depth south of the Azores consists of a series of undulations at various scales [see *Detrick et al.*, 1995]. The question then arises how the "regional gradient" in geochemistry is influenced by segmentation. Is the gradient regular, or is it undulating like the depth, or does it have other characteristics? In order to fully grasp the mechanisms involved in the creation of ocean crust and the distribution of mantle plume influence, the effects of segmentation on regional gradients need to be better understood.

[4] The gradients around plumes also provide a natural laboratory to explore the relationships between ridge segmentation and magma supply. Two end-member models for the formation of segments are "multiple supply" and "central supply." Multiple supply [e.g., *Bender et al.*, 1984; *Langmuir et al.*, 1986, 1977] calls on vertical upwelling of magma from the mantle to the crust, with volcanic eruptions sourced along the entire length of a ridge segment. Melt compositions then reflect the composition of the mantle and the extent of melting as it varies (or not) along the segment. Central supply [e.g., *Schouten et al.*, 1985] equates ridge segments with central volcanoes, akin to Hawaii, with a single central pipe as the source of dike-fed eruptions that fill the entire segment. The "multiple supply" model also allows for greater extents of volcanism at segment centers compared to segment ends, but nonetheless calls upon distributed magmatism along the length of the segment rather than a point source injection.

[5] These two views of ocean ridge magmatism have a long history. Central injection is supported by detailed studies of volcanoes on rift zones of Hawaii and Iceland [*Parfitt*, 1991; *Gudmundsson*, 1998], by the recent evidence for lengthy dike propagation on the Juan de Fuca ridge [*Embley et al.*, 1995; *Fox et al.*, 1995] and by the ubiquity of dikes as a fundamental feature of the ocean crust [*Curewitz and Karson*, 1998]. *Michael et al.* [1989] noted geochemical distributions along strike that suggested lateral injection of magma from central segment highs toward segment edges along the Explorer Ridge. Central injection has also been inferred from recent seismic studies [*Hooft et al.*, 2000; *Magde et al.*, 2000], from geophysical modeling [*Magde and Sparks*, 1997], and from systematic variations in magma temperature with distance from segment centers [*Thompson and Melson*, 1972; *Schilling and Sigurdsson*, 1979; *Natland and Melson*, 1980; *Lawson et al.*, 1996]. The common occurrence of mantle Bouguer anomaly (MBA) lows at the centers of ridge segments implies greater crustal thickness and hence preferential emplacement of magma to the segment center [e.g., *Kuo and Forsyth*, 1988].

[6] Multiple injection also has convincing evidence. Geochemical studies of basalts from the FAMOUS area [*Langmuir et al.*, 1977; *White and Bryan*, 1977; *leRoex et al.*, 1981] showed that individual cones in the middle of the rift valley represent discrete melts from the mantle. *Bender et al.* [1984] suggested a "transform fault effect" of lower extents of melting at segment ends as compared to segment centers, subsequently supported by modeling of mantle flow [*Morgan and Forsyth*, 1988]. Variations in degree of melting systematically distributed within a segment require multiple supply. A study by *Niu and Batiza* [1994] supported the inference of systematic segment scale changes in extent of melting, requiring vertical transport of different melts to crustal levels. In their study of basalts from the MARK area south of the Kane fracture zone, *Reynolds and Langmuir* [1997] argued that melts from the segment edges are independent of those from the segment center. These lines of evidence support multiple supply of magma along strike, which in turn requires limited focusing. Of course it is likely that no single

model applies to all segments. Some may be centrally and others multiply supplied, and these characteristics may vary with time.

[7] Segmentation within a regional gradient provides opportunities to address these models. Multiple supply would be necessary if geochemical gradients were present within the segments. Central supply would be implicated by more homogeneous parental magmas within segments, and a step function in chemistry between segments. Variable magmas could still exist in a centrally supplied segment, but the variation would not be systematically distributed along strike.

[8] In this paper we address these issues with a detailed petrological study of the Lucky Strike and Menez Gwen segments on the Mid-Atlantic Ridge (MAR; Figure 1). These segments are within the geochemical and bathymetric gradient just south of the main Azores platform and have been well sampled along most of their length. Several active seismic and refraction studies at Lucky Strike provide important physical constraints [e.g., *Singh et al.*, 2006; *Combier*, 2007; *Seher et al.*, 2010]. To better place the data in the context of the regional gradient in composition, we also report data for samples from the nearby "plume" segments KP-2 and -3 on the Azores platform that had limited existing inductively coupled plasma–mass spectrometry (ICP-MS) trace element data (see Figure 1; segment nomenclature is from *Detrick et al.* [1995]).

2. Regional Setting

[9] The Menez Gwen (KP-5) and Lucky Strike (PO-1) segments are the second and third segments south of the bathymetric summit that occurs adjacent to the Azores islands near 39°N (Figure 1). The segments are separated by the Pico transform fault.

[10] The Lucky Strike segment (Figure 1) is 65 km long and rectangular (11–12 km wide) with a mean depth of ~2580 m. One of the largest seamounts along the MAR is found in the center of the segment, rising to 1660 m depth. Several ridges extend from the seamount toward the north and south [*Langmuir et al.*, 1997; *Parson et al.*, 2000], suggesting dike-fed fissure systems. The seamount summit is filled by young lava flows that overlie older lavas that make up the main edifice [*Fouquet et al.*, 1995], and is the site of the Lucky Strike hydrothermal field [*Langmuir et al.*, 1997]. A large negative MBA near the central part of the segment [*Detrick et al.*, 1995] is consistent with thicker crust at the segment center (~6 km) than the segment ends (~4 km). An axial magma chamber (AMC) has been seismically detected 3.4 km beneath the central volcano, extending for ~6 km along axis [*Singh et al.*, 2006; *Combier*, 2007]. Recent microseismic experiments indicate that the brittle lithosphere thickens from ~6.5 km at the segment center to more than 10 km at the segment ends [*Dusunur et al.*, 2009].

[11] The Menez Gwen segment, just north of Lucky Strike (Figure 1), has a length of 64 km with a central bathymetric high that also hosts high-temperature hydrothermal activity [*Fouquet et al.*, 1995]. It is shallower than Lucky Strike overall (mean depth of ~1620 m), with a large volcanic edifice that occupies most of the segment length [*Ondréas et al.*, 1997]. These characteristics are consistent with its closer proximity to the main Azores platform. Young lava flows have been seen during dives within the graben at the volcanic summit [*Ondréas et al.*, 1997].

3. Sampling and Analytical Techniques

[12] The samples were collected by dredges, wax-rock cores and by the submersible Alvin during cruises AII127, AII129–6 and K145–19. In both segments, the highest density sampling occurred near the central region containing the hydrothermal vent (Figure 1). Nearly all of the samples studied were basaltic glass, but aphyric rocks were analyzed when glass was unavailable. Unaltered pieces of rock and glass chips for chemical analyses were handpicked under a microscope and cleaned ultrasonically in methanol for 20 min.

[13] Major elements were measured using a Cameca SX100 electron microprobe (EMP) at the American Museum of Natural History. A defocused beam resulting in an 8–10 μm spot size was used. The samples were analyzed at 15kV using two different running conditions. First, to minimize volatilization of K_2O and Na_2O, a low beam current of 5 nA with an 80 s count time was used. The beam current was then increased to 20 nA with a 30 s count time for SiO_2, CaO, MgO, FeO and a 60 s count time for Al_2O_3, TiO2, MnO, and P_2O_5. Each probe mount disk included an internal monitor standard, JDF-D2. This internal glass standard was analyzed (5 analytical spots) after every 25 analytical spots to monitor instrumental drift over time. Individual analyses reported in Table S1 in the auxiliary material are averages of 5 analytical spots normalized to JDF-D2, for which values are also reported.[1]

[1] Auxiliary materials are available in the HTML. doi:10.1029/2010GC003446.

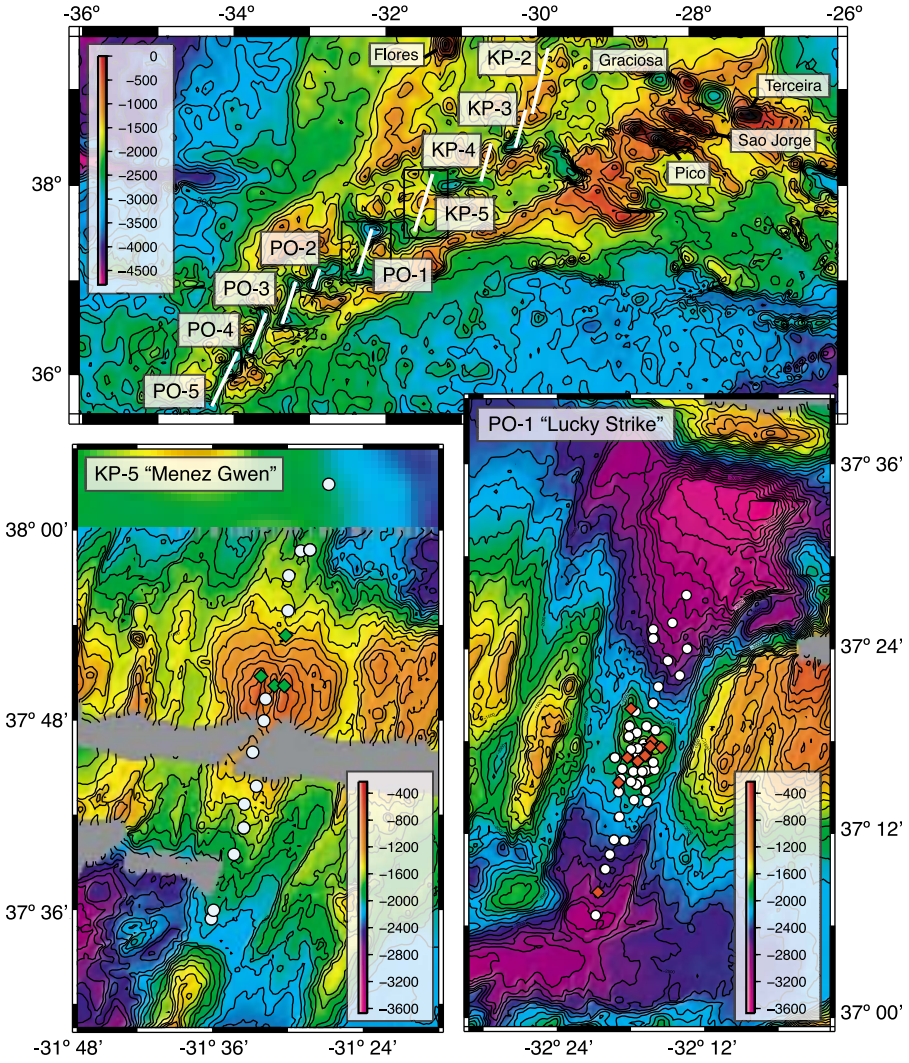

Figure 1. Bathymetric map of the northern Mid-Atlantic Ridge, with detailed maps of the Lucky Strike (PO-1) and Menez Gwen (KP-5) segments showing the location of samples in this study. Labeled segments (indicated by white lines in regional map) follow the nomenclature of *Detrick et al.* [1995]. Note that in both segments nearly all enriched samples (shown in diamonds) are near the central volcanic edifice. A multibeam bathymetry grid (300 m spacing) [*Cannat et al.*, 1999; *Escartín et al.*, 2001] was used for the detailed maps. Global multiresolution bathymetry as compiled by *Ryan et al.* [2009] was used for the regional map (bathymetry in meters).

Analytical uncertainties were obtained from replicate measurements of JDF-D2. The precision (2σ RSD) for SiO_2, TiO_2, Al_2O_3, MgO, FeO and CaO is better than 2%. The precision for K_2O and Na_2O is ~6%, and for MnO and P_2O_5 ~10%.

[14] Trace elements were measured by solution nebulized–inductively coupled–mass spectrometry and laser ablation–inductively coupled–mass spectrometry (SN-ICP-MS and LA-ICP-MS) at Lamont-Doherty Earth Observatory (LDEO) and by SN-ICP-MS at Harvard University (selected results in Table 1; full results in Table S2). Due to detection limits, different sets of elements are reported for each method and institution. For SN-ICP-MS, 50 mg of handpicked rock or glass chips were digested in an HF:HNO_3 mixture. Two dilutions were run (1:2K and 1:10K) at LDEO and one dilution was run at Harvard (1:5K) using a matrix solution of 0.2N HNO_3 with Ge (10 ppb), In (3 ppb), Tm (3 ppb) and Bi (3 ppb) as internal standards for drift correction. Measurements were obtained on a VG Plasma Quad2+ at LDEO and on a Thermo X series quadripole at Harvard. Standard powders BHVO-2, DNC-1, JB-2 and W-2 as well as two in-house standards (powdered MAR and handpicked glass chips of VE-32) were used to generate calibration curves (standard values in

Table 1 (Sample). Representative ICP-MS Analyses of Trace Element Concentrations of Glassy Basalts From Segments KP-3, -5, and PO-1[a] [The full Table 1 is available in the HTML version of this article]

Detrick Segment	Sample Name	Group Name	Latitude	Longitude	TE Ref	Li	Be	Sc	Ti	V	Cr
KP-5	AII0127-1-017-005	Enriched	37.836	−31.518	Harvard	3.9	0.60	44.5	1.30	256	390
KP-5	AII0127-1-017-003(A)	Enriched	37.836	−31.518	Harvard	3.7	0.65	39.9	1.30	237	346
KP-5	AII0127-1-R048	Enriched	37.889	−31.503	Harvard	3.9	0.65	39.5	1.30	240	374
KP-5	AII0127-1-R046	Transitional	37.711	−31.558	Harvard	5.8	0.49	42.0	1.33	303	56
KP-5	AII0127-1-018-001	Transitional	37.979	−31.471	Harvard	4.2	0.35	47.2	0.95	254	109
KP-5	AII0127-2-034-002	Transitional	37.590	−31.602	Harvard	5.3	0.46	43.1	1.16	287	66
KP-5	AII0127-2-033-002	Transitional	38.048	−31.446	Harvard	5.4	0.43	41.8	1.13	273	65
PO-1	AII0129-6 2604-3	Enriched	37.296	−32.272	LDEO			42.4		249	430
PO-1	AII0127-1-R041	Enriched	37.284	−32.281	Harvard	4.6	0.54	42.8	1.34	258	491
PO-1	AII0127-2-R116-002	Enriched	37.278	−32.291	Harvard	4.2	0.56	42.4	1.22	235	848
PO-1	AII0129-6-002-001	Transitional	37.285	−32.281	Harvard	4.8	0.36	42.3	1.07	273	77
PO-1	AII0127-2-R108-001	Transitional	37.316	−32.279	Harvard	4.4	0.31	42.9	0.95	258	100
PO-1	AII0127-1-015-001	Transitional	37.291	−32.283	Harvard	4.8	0.35	39.8	0.99	253	74
PO-1	AII0127-2-037	Transitional	37.256	−32.300	Harvard	4.3	0.34	42.1	0.94	238	284
KP-3	AII0127-1-021-003	n/a	38.491	−30.265	Harvard	6.1	1.40	28.5	2.08	258	75
	AII0127-1-021-003 Duplicate	n/a	38.491	−30.265	LDEO						
KP-5	AII0127-1-017-005	Enriched	37.836	−31.518	Harvard	3.9	0.60	44.5	1.30	256	390
	AII0127-1-017-005 Duplicate	Enriched	37.836	−31.518	LDEO						
PO-1	AII0127-2-036-020	Transitional	37.256	−32.288	Harvard	4.8	0.41	38.9	1.08	250	38
	AII0127-2-036-020 Duplicate	Transitional	37.256	−32.288	LDEO	4.5					

[a]Concentrations in ppm except for Ti and Mn, which are in wt. %.

Table S2). To ensure consistency between laboratories, certain samples were analyzed at both LDEO and Harvard (duplicates shown in Table 1).

[15] LA-ICP-MS analyses were performed on the same mounts used for the electron microprobe analyses using a Merchantech EXCIMER LASER (193 nm wavelength) connected to the VG Plasma Quad2+. This technique was useful for samples with limited glass or rock available. A 90–100 μm spot size was used with settings of 23–25 kv, resulting in energies of ~100 mJ. The ablation cell was flushed with a helium carrier gas using a flow rate of ~0.8 l/min. The precision for trace elements measured in this study is better than 5% for all elements except for U, Th and Pb measured at LDEO (both LA and SN) with precisions of 10% or better (2σ).

[16] For isotopes, the handpicked rock and glass chips were leached for 20 min with 8N HNO_3 and then rinsed with quartz-distilled water. Samples were digested using a HF:HNO_3 mixture in Teflon beakers. The Sr, Nd and Pb isotopes were measured from a single digestion that was run through progressive columns to isolate the element of interest. For samples with limited material, Sr and Nd or only Sr isotopes were determined. The isotopes were measured by TIMS on a VG Sector 54 multicollector at LDEO (results in Table 2). Sr and Nd isotopes were measured in dynamic mode. Sr isotopic values were corrected to an $^{87}Sr/^{86}Sr$ value of 0.710235 for NBS 987. Our measured value for NBS 987 $^{87}Sr/^{86}Sr$ was 0.710255 (2×10^{-5} 2σ). The Nd analyses were corrected using the JNDi standard ($^{143}Nd/^{144}Nd = 0.512115$). The average measured value was 0.512096 (2.1×10^{-5} 2σ). The Pb isotope data were collected in static mode using a double spike method for calibration. Both the samples and the NBS-981 standard were spiked with a ^{204}Pb and ^{207}Pb mixture. The double spike corrected values for NBS 981 were $^{206}Pb/^{204}Pb = 16.937$ (3.5×10^{-3} 2σ), $^{207}Pb/^{204}Pb = 15.490$ (4.7×10^{-3} 2σ), and $^{208}Pb/^{204}Pb = 36.691$ (1.4×10^{-2} 2σ). The measured values were then corrected to the values reported by *Todt et al.* [1996].

4. Results

[17] We report 110 new major element analyses, 79 new trace element analyses and 27 new isotope analyses in this study (representative trace element analyses in Table 1; isotope analyses in Table 2; all analyses reported in Tables S1 and S2). "New" analyses were mostly on new samples, but in certain cases were reanalyses (or supplementary analyses where only limited published trace element data existed) of previously measured samples. We report 65 new major element analyses complemented by 46 trace element analyses on samples from Lucky Strike. A selected subset (n = 27) of samples was also analyzed for Sr, Nd and/or Pb isotopes. For the

Table 2. Sr, Nd, and Pb Isotope Ratios of Samples From Lucky Strike Segment (PO-1)

Sample Name	Group Name	Latitude	Longitude	$^{87}Sr/^{86}Sr$	$^{143}Nd/^{144}Nd$	$^{206}Pb/^{204}Pb$	$^{207}Pb/^{204}Pb$	$^{208}Pb/^{204}Pb$
AII0129-6-R016	Transitional	37.161	−32.335	0.702892	0.513120	18.837	15.530	38.434
AII0127-1-015-001	Transitional	37.291	−32.283	0.702915	0.513126	18.856	15.530	38.430
AII0129-6-R005	Transitional	37.309	−32.292	0.702932	0.513115	18.929	15.538	38.501
AII0127-2-R105	Transitional	37.291	−32.300	0.702967	0.513129	18.946	15.549	38.551
AII0127-2-R107	Transitional	37.312	−32.267	0.702941	0.513113	18.812	15.533	38.419
AII0129-6 2602–3	Enriched	37.294	−32.274	0.703066	0.513022	19.224	15.569	38.757
AII0127-2-R108-001	Transitional	37.316	−32.279	0.702935	0.513127	18.967	15.549	38.567
AII0127-1-R041	Enriched	37.284	−32.281	0.703083	0.513081	19.243	15.574	38.784
AII0127-1-R040	Transitional	37.218	−32.316	0.702937	0.513112	18.975	15.581	38.585
AII0127-2-R103-001	Transitional	37.253	−32.293	0.702964	0.513140	18.878	15.539	38.479
AII0127-2-R113-001	Transitional	37.411	−32.270	0.702874	0.513172	18.807	15.528	38.409
AII0127-2-R110	Transitional	37.359	−32.263	0.703020	0.513122	18.910	15.539	38.492
AII0127-1-016-001	Transitional	37.458	−32.225	0.702925	0.513116	18.896	15.538	38.467
AII0127-2-R116-002	Enriched	37.278	−32.291	0.703098	0.513031	19.254	15.571	38.779
AII0127-2-R104	Transitional	37.267	−32.285	0.702910	0.513106			
AII0129-6 2604-3	Enriched	37.296	−32.272	0.703125	0.513021			
AII0127-2-038-004	Transitional	37.111	−32.348	0.702925	0.513118			
AII0127-2-036-020	Transitional	37.256	−32.288	0.702925	0.513131			
AII0129-6-003	Transitional	37.335	−32.289	0.703023	0.513141			
AII0127-2-R117-001	Transitional	37.236	−32.296	0.702888	0.513121			
AII0127-2-R112-001	Transitional	37.400	−32.224	0.703045	0.513139			
AII0127-2-035	Transitional	37.421	−32.270	0.702915	0.513117			
AII0127-2-R111-001	Transitional	37.371	−32.234	0.702989	0.513082			
AII0127-2-R109-001	Transitional	37.341	−32.270	0.702972	0.513126			
AII0129-6-002-001	Transitional	37.285	−32.281	0.702932				
AII0129-6 2602-5b	Enriched	37.300	−32.272	0.703145				
AII0127-1-R039	Enriched	37.136	−32.345	0.702941				

Menez Gwen segment we report 23 new major element analyses and 17 new trace element analyses. We also present 22 new major element analyses and 16 new trace element analyses from segments KP-2 and -3 on the Azores platform for comparative purposes. Isotopic data from *Dosso et al.* [1999] on many of the same Menez Gwen and KP-2 and -3 samples for which we have new major and trace element data supplement our isotopic analyses from Lucky Strike.

4.1. Major Elements

[18] At the outset it is necessary to be clear about terminology for describing MORB compositions. The terms "enriched" and "depleted" have become common parlance in ocean ridge studies. Normal MORB (N-MORB) have $La/Sm_N < 1$, $K_2O/TiO_2 < 0.11$ and isotopic compositions reflecting long-term depletion in the more incompatible element (e.g., high $^{143}Nd/^{144}Nd$, low $^{87}Sr/^{86}Sr$, low $^{206}Pb/^{204}Pb$). Enriched MORB (E-MORB) are enriched in the highly incompatible elements (e.g., $La/Sm_N > 2$, $K_2O/TiO_2 > 0.2$) and their isotope ratios also reveal less long-term depletion of the more incompatible element (e.g., low $^{143}Nd/^{144}Nd$, high $^{87}Sr/^{86}Sr$, high $^{206}Pb/^{204}Pb$). Transitional MORB (T-MORB) are intermediate between the two. Ultimately there is a continuity of compositions, so such names are arbitrary. In comparing samples, terms such as "more enriched" and "less enriched" are clear.

[19] Chemical compositions of basalt samples from Lucky Strike and Menez Gwen are all enriched relative to N-MORB, but separate into two distinct groups in major elements (Figure 2). Both Lucky Strike and Menez Gwen contain a T-MORB group (hereafter referred to as "transitional") characterized by K_2O contents between 0.12 and 0.23 wt.%, TiO_2 from 0.89 to 1.01 wt.%, FeO between 8.74 and 9.31 wt.%, Al_2O_3 from 14.84 to 15.09 wt.% and SiO_2 ranging from 50.72 to 51.7 wt.% for MgO between 8.72 and 8.04 wt.%. These major element characteristics are very similar to most samples from the well-studied FAMOUS segment ~70 km to the south [e.g., *Bryan and Moore*, 1977; *Bryan*, 1979; *Melson et al.*, 2002]. In contrast, Lucky Strike and Menez Gwen also contain a true E-MORB group (called "enriched"), distinguished by distinctly higher K_2O (0.58–0.67 wt.%), higher TiO_2 (1.22–1.35 wt.%), lower FeO (6.99–7.95 wt.%), higher Al_2O_3 (15.58–16.12 wt.%) and lower SiO_2 (48.93–50 wt.%) for the same MgO range. These samples are also more vesicular than the transitional samples, indicative of higher initial volatile contents.

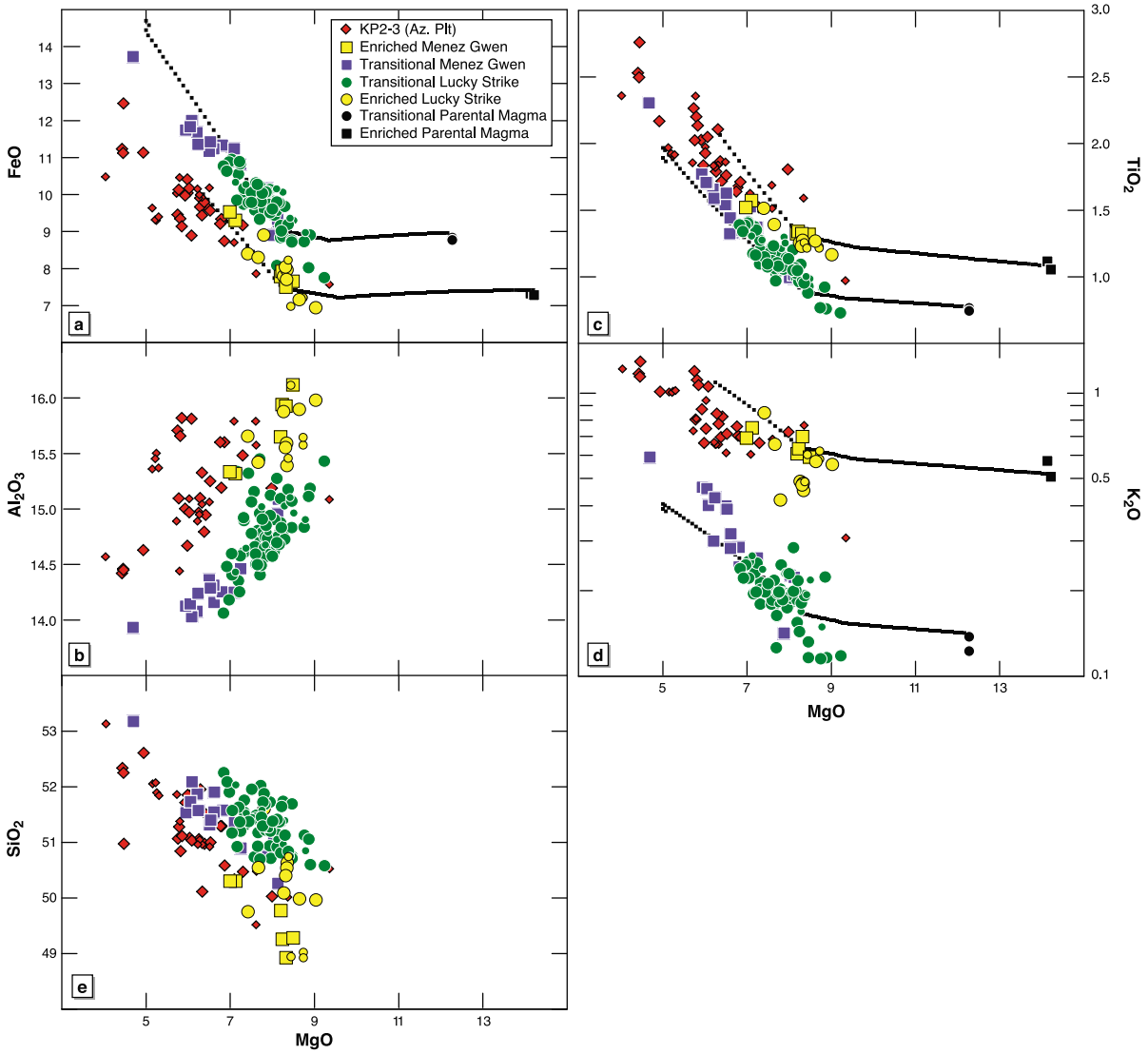

Figure 2. (a–e) FeO, Al_2O_3, TiO_2, K_2O, and SiO_2 versus MgO. Smaller symbols indicate data already published [*Langmuir et al.*, 1997; *Cooper et al.*, 2004]. At both Menez Gwen and Lucky Strike, there are two distinct groups in major elements, an enriched group and a transitional group. Multiple parental magmas are required to explain the variability observed at a given MgO content (represented by the black squares (showing extent of melting (F) of 6.5% and 7.5%) and circles (F of 7.2% and 8.7%)). The variability within the groups, however, shows a large effect of low-pressure fractionation (representative LLDs from Bezos et al., manuscript in preparation, 2011; no LLDs are shown for SiO_2 and Al_2O_3 because they are not included in our major element model). Also shown for comparison are samples from segments KP2–3 on the Azores platform (data from this study and smaller symbols from *Sigurdsson* [1981] and *Melson et al.* [2002]). The enriched groups from both segments are quite similar to the Azores platform lavas.

[20] Chemical variation within the groups is also evident. Low-pressure crystal fractionation has played an important role in diversifying the lava compositions (Figure 2; calculated liquid lines of descent from hBasalt (A. Bezos et al., manuscript in preparation, 2011)), but there are also differences within each group that cannot be attributed to fractionation. For example, $K_{8.0}$, the concentration of K_2O corrected for fractionation to 8% MgO, varies from 0.12 to 0.29 for Lucky Strike transitional samples, and these variations correlate positively with $Ti_{8.0}$. The variations within each group are small, however, relative to the contrast between the transitional and enriched groups.

[21] There are other important aspects to note in the major element data. The MgO contents of transitional

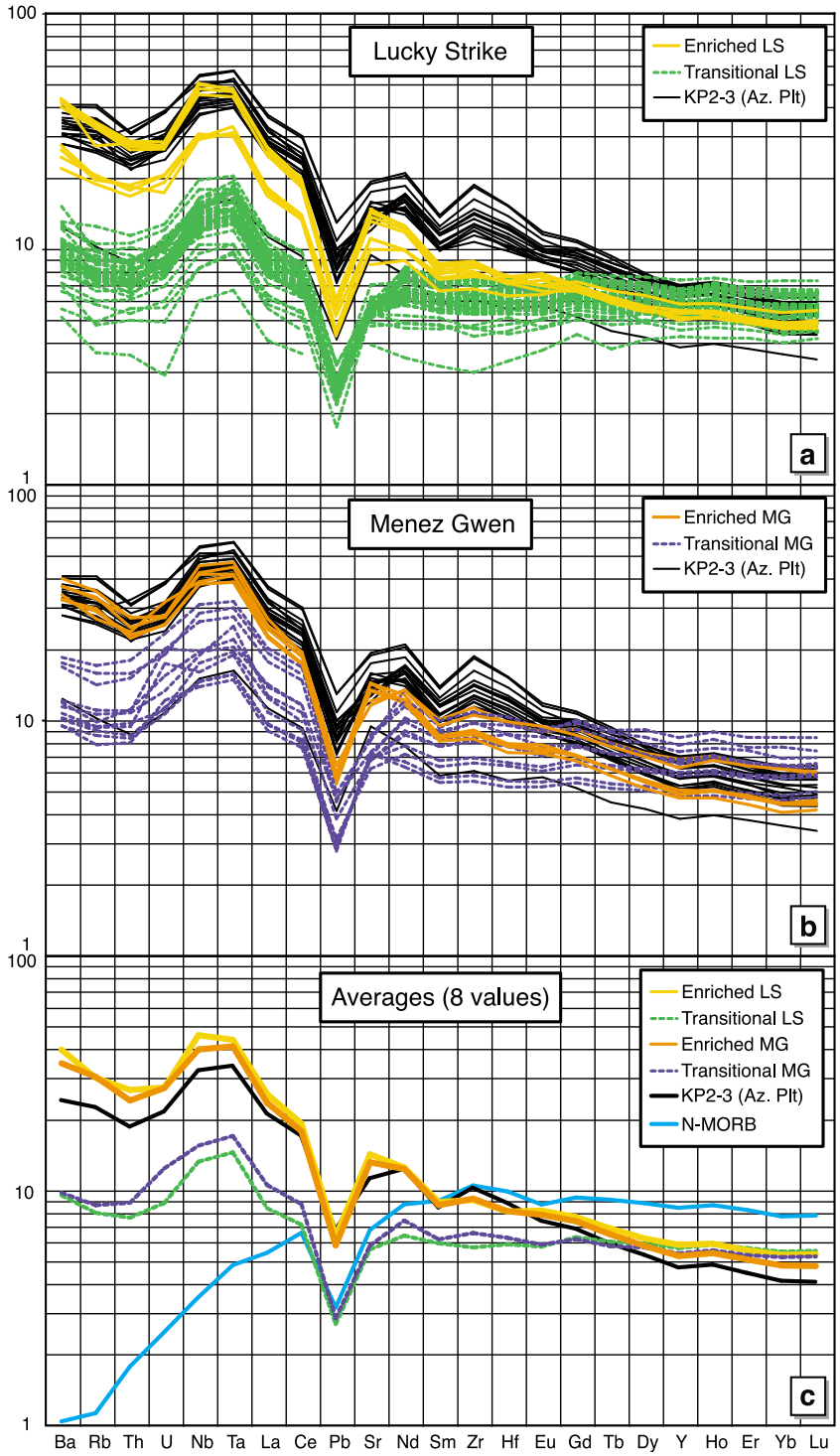

Figure 3. (a–b) Pyrolite-normalized spidergrams [*McDonough and Sun*, 1995] showing the trace element patterns of enriched and transitional samples from both segments, with lavas from KP2–3 for comparison. Note the strong enrichment in highly incompatible elements associated with the enriched groups and the crossing patterns of the enriched and transitional groups in the REE. (c) Average trace element patterns of the enriched and transitional groups at each segment compared to an N-MORB from the MAR [*Donnelly et al.*, 2004] and the average of samples from KP2–3 (concentrations corrected to 8 wt.% MgO; details on correction are given in the auxiliary material). All samples from Menez Gwen and Lucky Strike are enriched relative to N-MORB in the highly incompatible elements, but the enriched groups are more extremely enriched, with concentrations nearly identical to the Azores platform lavas.

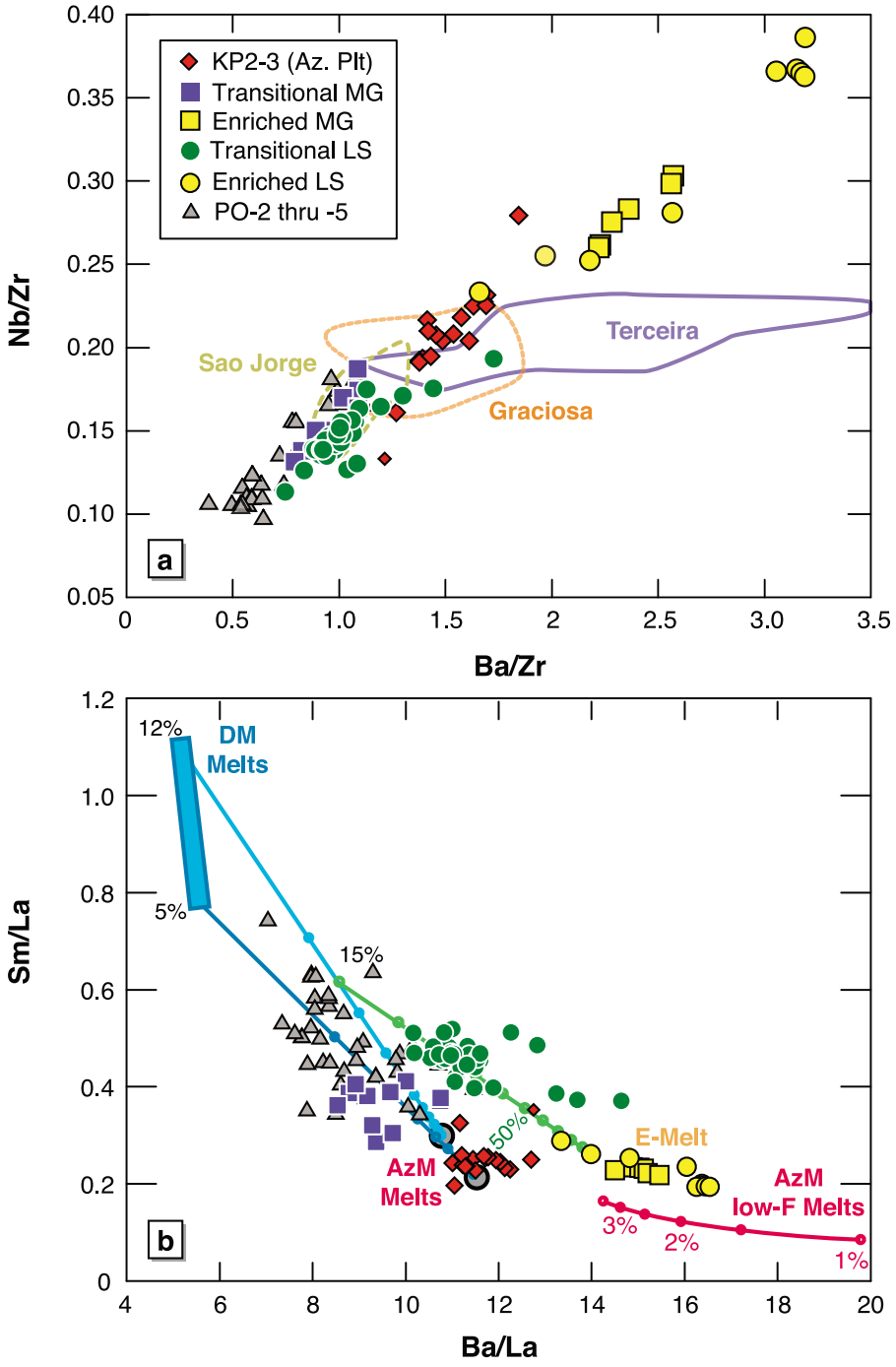
KP2-3 (Az. Plt)
Transitional MG
Enriched MG
Transitional LS
Enriched LS
PO-2 thru -5
Nb/Zr
Ba/Zr
Sao Jorge
Terceira
Graciosa
a
Sm/La
Ba/La
12%
DM
Melts
5%
15%
50%
AzM
Melts
E-Melt
AzM
low-F Melts
3%
2%
1%
b

Figure 4

samples decrease northward, with very few samples from Menez Gwen having as high MgO as the average sample from Lucky Strike. The average $Si_{8.0}$ (SiO_2 corrected to 8% MgO) of transitional lavas also decreases northward from 51.24 at Lucky Strike to 50.85 at Menez Gwen. The enriched samples from Menez Gwen and Lucky Strike are virtually identical in their major element composition and have higher MgO, and much higher Mg# (defined as (Mg/(Mg + Fe*)) × 100; Fe expressed as total Fe), than the average transitional sample from the same segment. Their major element characteristics are more similar to (but less fractionated than) those of Azores platform lavas (Figure 2).

[22] To be consistent with the gradient in enrichment south of the Azores, Menez Gwen samples would be more enriched than those from Lucky Strike, since Menez Gwen is closer to the Azores. Indeed, the transitional lavas exhibit such a "regional gradient," with Menez Gwen having a higher average K_2O/TiO_2 ratio than Lucky Strike, although there is substantial variability within each segment. A more striking aspect of the data, however, is that the enriched groups of both segments have samples with higher K_2O/TiO_2 ratios than the Azores platform lavas and their extreme values are very similar. This suggests that the processes giving rise to the enriched groups may be alike at both segments.

4.2. Trace Elements

[23] Trace elements confirm and expand the observations from the major elements. The more enriched groups in both segments have strongly elevated concentrations of the highly incompatible trace elements such as Ba, Rb, Th, Nb and U (Figures 3a and 3b). On a pyrolite-normalized spidergram (values from *McDonough and Sun* [1995]), the enriched samples show a steeply sloping pattern extending to the heavy rare earth elements (HREE) that crosses over the somewhat flatter pattern in the transitional samples. The enriched samples also have normalized patterns that are more concave upward through the light rare earth elements (LREE), evident when comparing their average $(La/Sm)_N$ (2.78) to that of the transitional samples (1.56).

[24] Average trace element compositions of the enriched and transitional samples from each segment are also shown in a pyrolite-normalized diagram (Figure 3c), along with the average composition of Azores platform lavas and an N-MORB from the MAR [*Donnelly et al.*, 2004] for comparison. The trace element concentrations of all samples were corrected to 8 wt.% MgO prior to averaging to eliminate the effects of crystal fractionation (details on the correction given in the auxiliary material). Key observations include the following: (1) all samples are enriched relative to N-MORB in the highly incompatible elements due to the influence of the Azores hot spot [*Schilling et al.*, 1983; *Schilling*, 1975]; (2) the enriched groups are significantly more enriched and their trace element concentrations and patterns are similar to the Azores platform samples; (3) the Menez Gwen transitional group has elevated concentrations relative to the Lucky Strike transitional group in the highly to moderately incompatible elements; and (4) the middle to heavy REE concentrations of all groups are lower than those of the N-MORB.

[25] The enriched basalts in the Lucky Strike, Menez Gwen and Azores platform segments have important differences. For example, enriched basalts at Menez Gwen and Lucky Strike have higher ratios of highly incompatible to moderately incompatible elements (e.g., Nb/Zr, Th/Sm, Ba/La, Rb/Hf) than the Azores segments (Figure 4a), but lower moderately incompatible element ratios (e.g., Zr/Y,

Figure 4. (a) Nb/Zr versus Ba/Zr for samples from Lucky Strike, Menez Gwen, KP2–3, and other segments farther south (segments PO-2 through PO-5). ICP-MS data from PO-2 through 5 were taken from *Yi et al.* [2000], *Nishio et al.* [2007], *Chauvel and Blichert-Toft* [2001], *Cooper et al.* [2004], and A. Gale unpublished data, 2010. Seven complete ICP-MS analyses have been published on KP2–3, Menez Gwen, and Lucky Strike; five of them are from *Yi et al.* [2000] and *Cooper et al.* [2004] and are from samples we also analyzed. As our analyses agree very well, we show only our data for these samples. The two remaining analyses from *Chauvel and Blichert-Toft* [2001] and *Cooper et al.* [2004] appear in Figure 4 (smaller symbols). Fields are also shown for the islands of Terceira, Sao Jorge, and Graciosa (data were taken from GeoROC). The enriched samples are much higher than the Azores platform and island lavas in the highly incompatible trace element ratios. (b) Sm/La versus Ba/La. All Lucky Strike samples plot off the main trend between the N-MORB and the Azores platform (AzM) toward a higher Ba/La ratio. The enriched samples have the most extreme Ba/La ratios, higher than the Azores platform lavas despite their similar Sm/La ratios. Also shown are three curves: the dark and light blue curves show the "regional gradient" between DM and AzM (dots are 10% increments) melted 5% and 12%, respectively; the green curve shows a mix between a "regional melt" with 15% Azores in the source and an enriched melt (E-Melt), and the red curve shows the field for low-F Azores melts in the garnet field between 1% and 3.5% (dots are 0.5% increments).

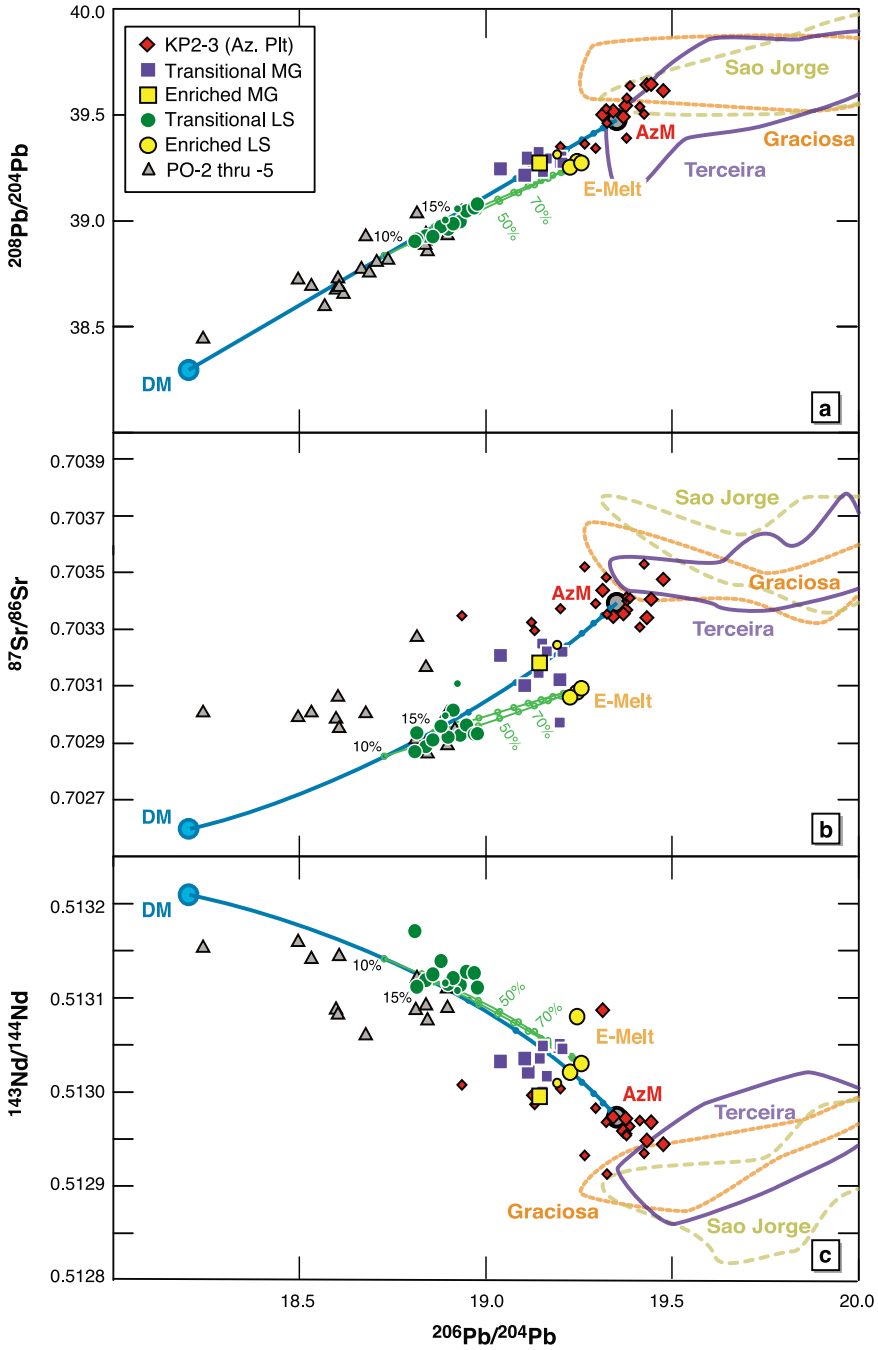

Figure 5. (a–c) The $^{208}Pb/^{204}Pb$, $^{87}Sr/^{86}Sr$, and $^{143}Nd/^{144}Nd$ versus $^{206}Pb/^{204}Pb$. Data are from this study and others [*Dosso et al.*, 1999; *Yu et al.*, 1997; *Chauvel and Blichert-Toft*, 2001; *Agranier et al.*, 2005; *Ito et al.*, 1987; *Frey et al.*, 1993; *Nishio et al.*, 2007]. Fields are also shown for the islands of Terceira, Sao Jorge, and Graciosa (data were taken from GeoROC). Isotope data from before 1985 are not shown. For consistency, all data were renormalized according to the normalization scheme given in section 3. For Lucky Strike, smaller symbols indicate isotope data from *Dosso et al.* [1999]. For Menez Gwen and KP2–3, smaller symbols indicate that we do not report ICP-MS data on the sample. All Lucky Strike samples form a linear trend pointing toward the Azores (AzM) in $^{208}Pb/^{204}Pb$ versus $^{206}Pb/^{204}Pb$. Within this general enrichment, however, enriched Lucky Strike samples are even more enriched isotopically than the transitional samples. The enriched Lucky Strike samples are also more similar in $^{208}Pb/^{204}Pb$ than in $^{87}Sr/^{86}Sr$ to the AzM, evidence for the low-F metasomatization of their mantle source. Menez Gwen samples are isotopically intermediate between Lucky Strike and AzM. Shown are the "regional gradient" (mixing curve for DM and AzM) and two green curves indicating the mixing between a regional melt with 10%–15% Azores and E-Melt, consistent with the trace element modeling for the transitional Lucky Strike samples.

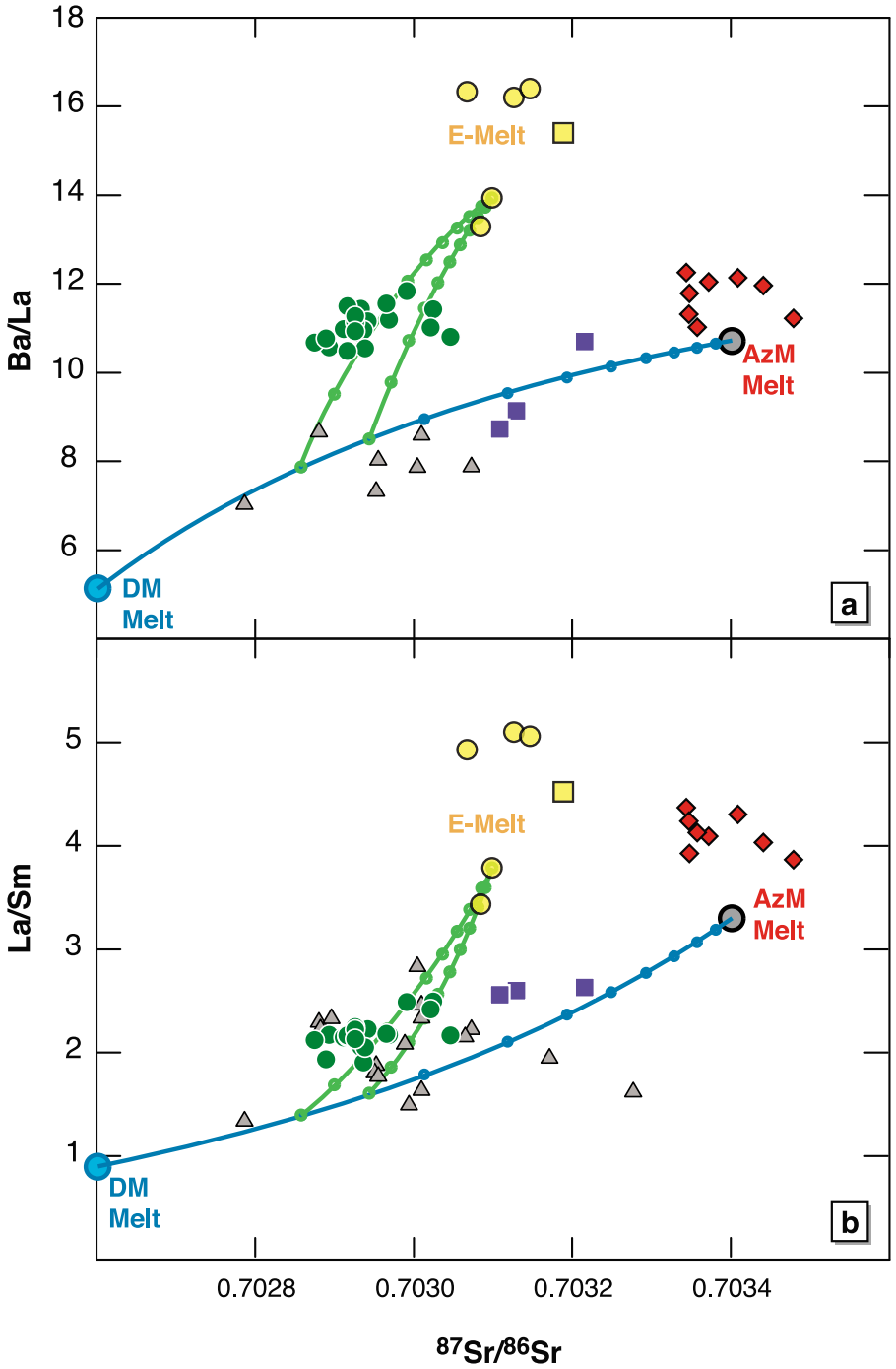

Figure 6. (a–b) Ba/La and La/Sm versus $^{87}Sr/^{86}Sr$. Symbols are as in Figures 4–5. For southern segments PO-2 through 5 for which no ICP-MS data were available on samples with measured isotopes, we show non–ICP-MS trace element data (same data sources as above). The enriched samples from both segments have as high or higher La/Sm and Ba/La than KP2–3 lavas, while having lower $^{87}Sr/^{86}Sr$ values. Again, the "regional" gradient and the mixing curves between a regional melt and E-Melt are shown; transitional Menez Gwen samples are on the regional gradient, whereas transitional Lucky Strike lavas show a deflection toward the E-Melt.

Sm/Yb). The trace element data also show a subtle distinction between the Menez Gwen and Lucky Strike enriched lavas, as the average Zr/Y and Sm/Yb increase from Lucky Strike to Menez Gwen.

[26] To sum up, both major and trace elements define two different groups of lavas, with enriched (E-MORB) and transitional (T-MORB) groups in each segment with distinctive compositions. The

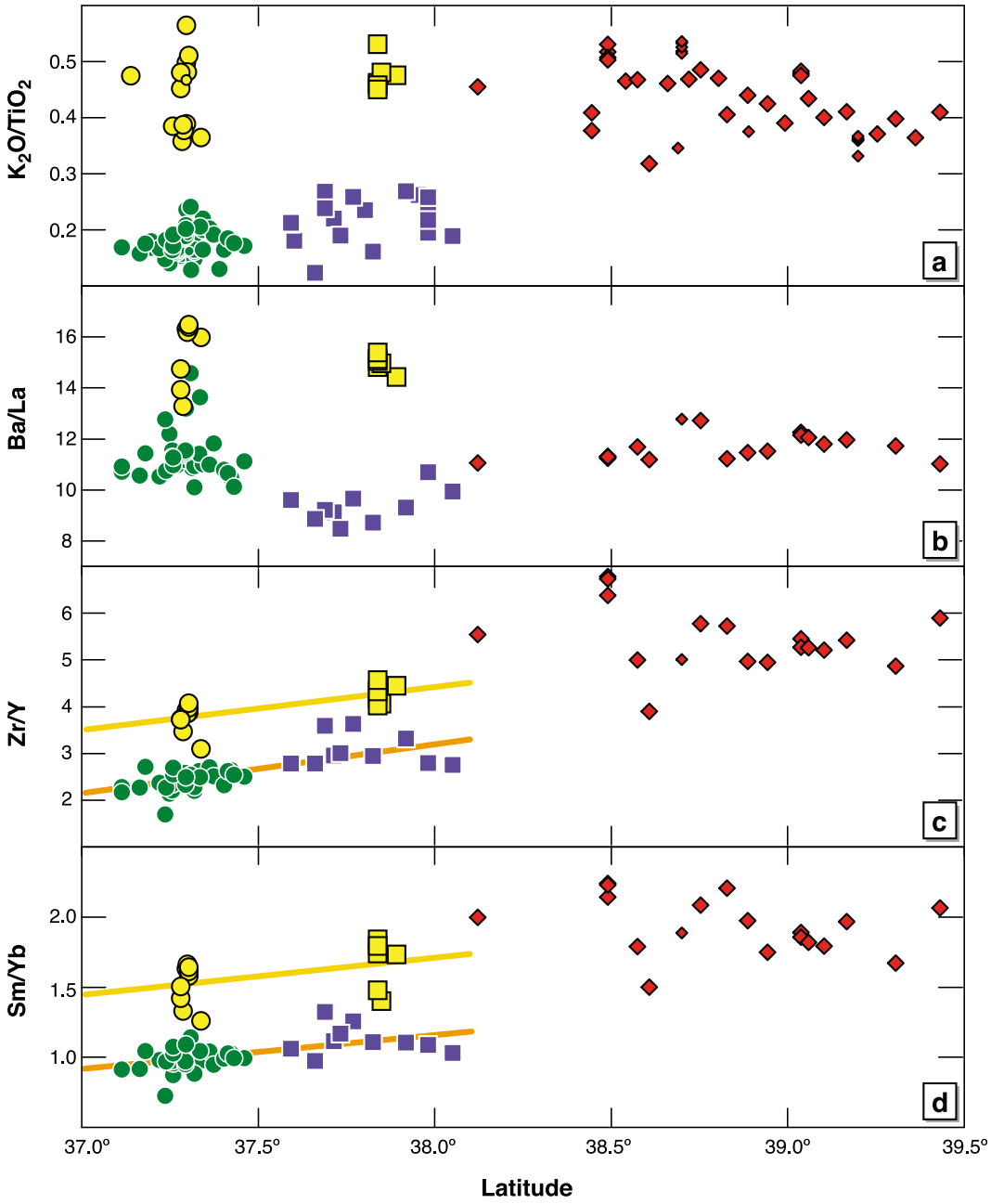

Figure 7. (a–d) K_2O/TiO_2, Ba/La, Zr/Y, and Sm/Yb versus latitude for the Lucky Strike, Menez Gwen, and KP2–3 segments. Symbols are as in Figures 4–6; errors on the ratios are smaller than the symbols. "Central spikes" are clearly visible in major and trace element ratios at Menez Gwen and Lucky Strike, with the enriched samples offset to higher values at the segment centers. Surprisingly, the average Ba/La of the transitional Lucky Strike samples is higher than that of Menez Gwen, while their average Zr/Y and Sm/Yb are lower. This highlights an amplified "low-F" signature at Lucky Strike, while the bulk Azores enrichment reflected in moderately incompatible elements is stronger at Menez Gwen. Zr/Y and Sm/Yb increase from Lucky Strike to Menez Gwen in the enriched samples, and they appear to increase continuously from southern Lucky Strike to northern Menez Gwen in the transitional group samples (calculated lines of best fit are shown).

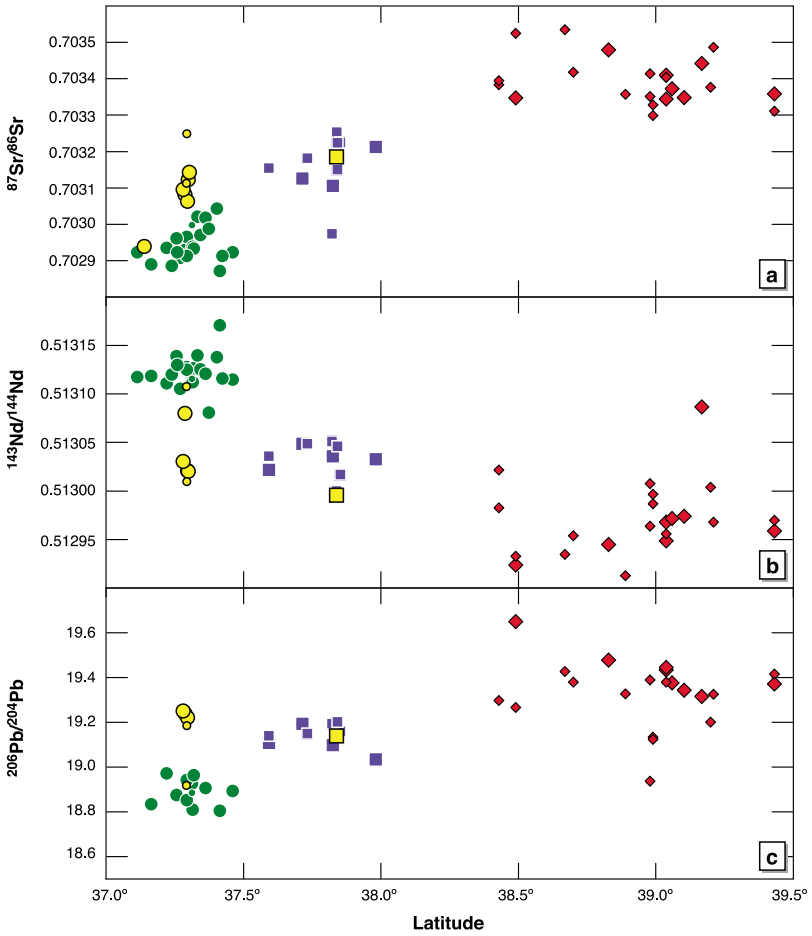

Figure 8. (a–c) The $^{87}Sr/^{86}Sr$, $^{143}Nd/^{144}Nd$, and $^{206}Pb/^{204}Pb$ versus latitude for Lucky Strike, Menez Gwen, and KP2–3 segments. Errors are smaller than the symbol size. "Central spikes" are also visible in isotopic ratios at Lucky Strike. Rather than the more gradual increase seen within segments in the moderately incompatible element ratios, there is a sharp jump in isotopic signature between the northernmost end of Lucky Strike and the southernmost end of Menez Gwen and no clear within-segment gradients.

enriched samples from both segments have very similar major elements, and highly incompatible to moderately incompatible element ratios that exceed those of the Azores platform lavas. Both groups also show gradients toward the Azores. The transitional samples show decreasing $Si_{8.0}$ and increasing incompatible element concentrations and moderately incompatible element ratios from Lucky Strike to Menez Gwen. The enriched samples show gradients in moderately incompatible element ratios. Both the existence of the distinct groups within each segment and their gradients need to be explained.

4.3. Isotopes

[27] This study combines new isotopic measurements for Lucky Strike with literature data from Menez Gwen and the Azores. All lavas from Menez Gwen and Lucky Strike are isotopically intermediate between depleted MORB mantle (DM) and the fields of the Azores islands (Figure 5). The regional gradient is reflected in the more enriched (e.g., higher $^{87}Sr/^{86}Sr$ and $^{206}Pb/^{204}Pb$, lower $^{143}Nd/^{144}Nd$) isotopic ratios of transitional Menez Gwen basalts compared to transitional Lucky Strike basalts. In the $^{208}Pb/^{204}Pb$ versus $^{206}Pb/^{204}Pb$ diagram, samples from Lucky Strike and Menez Gwen form a linear trend pointing toward the KP-2 and -3 lavas and certain Azores islands, implying that the source of isotopic enrichment is the Azores plume (Figure 5a).

[28] There are several notable features in the isotopic ratios of enriched samples. First, the isotopic ratios of the enriched Lucky Strike samples are more enriched than the transitional Lucky Strike samples. There is no clear isotopic difference between the measured Menez Gwen enriched sample and the transitional Menez Gwen lavas, but this was one analysis on a whole rock so we hesitate to infer too

much from this result. Second, the enriched Lucky Strike lavas are lower than Menez Gwen samples in $^{87}Sr/^{86}Sr$, but are actually higher in $^{206}Pb/^{204}Pb$. This peculiarity of Pb isotopes showing more extreme enrichment than the Sr isotopes of the enriched samples will provide constraints on the process involved. Third, the isotopes of enriched Lucky Strike and Menez Gwen samples are still less enriched than those of the Azores. This central feature of enriched samples with higher incompatible trace element ratios (e.g., Ba/La and La/Sm) than the Azores platform samples despite lower isotopic ratios (Figure 6) is a core observation that must be explained.

4.4. Enriched Samples Occur at Segment Centers

[29] In both segments the enriched samples occur near the center of the segment. In Figures 7 and 8, these "central spikes" are clearly visible in major element, trace element and isotopic ratios versus latitude plots. There also appear to be more intermediate samples at Lucky Strike, whereas at Menez Gwen the two groups remain quite distinct.

4.5. Complexities of the Regional Gradient

[30] The new data show that the regional gradient is not smooth. First, the enriched samples have higher highly incompatible trace element ratios than Azores platform samples. Second, transitional Lucky Strike samples have higher highly incompatible element ratios (e.g., Ba/La, Rb/La, Nb/La) relative to transitional Menez Gwen samples but lower moderately incompatible element ratios (e.g., K_2O/TiO_2, Zr/Y) and less radiogenic isotopic signatures (see Figures 5 and 7). These characteristics cause the Lucky Strike basalts to deviate from the smooth trend of enrichment between N-MORB and the Azores platform lavas exhibited by other segments south of the Azores (see Figure 4b). Finally, while the moderately incompatible element ratios of transitional samples show within-segment gradients of continuous increase from the southern end of Lucky Strike toward the northern end of Menez Gwen (Figures 7c and 7d), isotopes show no such gradient. Instead, there is a discrete step change from the isotopes of transitional Lucky Strike samples to the isotopes of transitional Menez Gwen samples (see Figure 8).

5. Discussion

[31] The absence of a simple regional gradient complicates discussion of issues of central and multiple supply and their relationship to segmentation. Before addressing the magma supply questions, the two distinct geochemical groups in each segment and the complexities of the regional gradient need to be understood.

5.1. Origin of the Enriched Samples From Segment Centers: General Framework

[32] There are two pieces of critical evidence for the origin of the enriched samples: (1) the dichotomy between the isotope and trace element systematics; (2) the higher highly incompatible element ratios in the enriched samples compared to the Azores platform lavas.

[33] Highly incompatible element ratios can be fractionated only by very low extents of melting, suggesting involvement of a "low-F" melt akin to what was proposed by *Donnelly et al.* [2004]. A low-degree (low-F) melt contribution from a garnet-bearing enriched "Azores source" (more details on Azores source below) could lead to the elevated incompatible element ratios of the enriched lavas. Such a low-F melt has (1) strongly enriched highly incompatible trace element abundances with very low HREE contents, (2) fractionated highly incompatible trace element ratios that are higher than the original Azores source and (3) an Azores isotopic signature. When this low-F melt is mixed with a more depleted component, the characteristics required by the enriched samples can be accounted for, including a negligible effect on the HREE and a very modest effect on moderately incompatible elements.

[34] Quantitative assessment of this process requires an estimate of the trace element content of the enriched Azores source. We must first consider whether the Azores islands or platform lavas (or both) are representative of a "true" Azores plume composition. The Azores plume has long been known to be chemically heterogeneous, in particular with regard to the island of Sao Miguel [e.g., *White et al.*, 1979; *Beier et al.*, 2007; *Widom et al.*, 1997; *Turner et al.*, 1997 and references therein]. Samples from the island of Terceira contain the most primitive He isotope ratios measured at the Azores ($^4He/^3He$ ~64,000) but a similar helium isotopic signature was found in KP-2, -3 MORB [*Moreira and Allegre*, 2002; *Moreira et al.*, 1999]. Lavas from the Azores islands of Terceira, Sao Jorge and Graciosa also overlap the most enriched basalts from the KP-2 and -3 segments in other isotopic and trace element ratios (shown in Figures 4a and 5). These lines of evidence suggest that the KP-2 and -3 lavas are representative of a "Regional Azores plume

Table 3. K_d's, Mantle Source Compositions, and Melting Reactions Used in the Modeling

	K_d Olivine/Melt	K_d Opx/Melt	K_d Cpx/Melt	K_d Gt/melt	Mantle Source 1	Mantle Source 2	Azores (AzM)	DM[a]	Average Metasomatized Mantle Source
Rb	0.000045	0.00045	0.0006	0.00001	0.0003		1.804	0.088	1.140
Sr	0.008	0.009	0.096	0.003	1.814		41.718	9.800	20.407
Y	0.007	0.025	0.421	2.8	1.606		4.885	4.070	2.053
Zr	0.0013	0.013	0.128	0.27	1.203		17.756	7.940	6.662
Nb	0.000041	0.0001	0.007	0.0042	0.002		3.054	0.211	1.867
Ba	0.000043	0.00004	0.00068	0.00001	0.001		25.100	1.200	15.601
La	0.00005	0.00005	0.042	0.001	0.012		2.024	0.234	1.033
Ce	0.00006	0.003	0.09	0.007	0.074		4.448	0.772	2.084
Nd	0.0002	0.007	0.19	0.06	0.147		2.582	0.713	1.108
Sm	0.0006	0.01	0.28	0.115	0.080		0.642	0.270	0.268
Eu	0.00015	0.013	0.355	0.5	0.037		0.237	0.107	0.098
Gd	0.00099	0.016	0.37	0.8	0.147		0.819	0.395	0.319
Tb	0.002	0.021	0.382	1	0.031		0.131	0.075	0.053
Dy	0.004	0.025	0.402	1.4	0.234		0.804	0.531	0.337
Ho	0.006	0.029	0.41	2	0.056		0.174	0.122	0.072
Er	0.0087	0.041	0.422	3.2	0.182		0.485	0.371	0.210
Yb	0.017	0.047	0.432	4.18	0.205		0.471	0.401	0.213
Lu	0.02	0.052	0.439	4.5	0.034		0.070	0.063	0.034
Hf	0.005	0.013	0.23	0.115	0.053		0.460	0.199	0.171
Pb	0.0003	0.0021	0.086	0.0003	0.003		0.180	0.023	0.059
Th	0.00005	0.00005	0.003	0.0015	0.00004		0.207	0.014	0.125
U	0.00005	0.00005	0.0052	0.027	0.00003		0.061	0.005	0.033
$^{87}Sr/^{86}Sr$							0.703400	0.702600	
$^{143}Nd/^{144}Nd$							0.512974	0.513210	
$^{206}Pb/^{204}Pb$							19.350	18.200	
$^{207}Pb/^{204}Pb$							15.610	15.507	
$^{208}Pb/^{204}Pb$							38.980	37.800	
MgO						36.70			39.00
FeO						8.30			6.34
Na_2O						0.21			0.21
TiO_2						0.10			0.12
K_2O						0.01			0.04
H_2O						0.02			0.03

	Source Mineralogy		Melting Reactions, Cpx Residual	
	Azores	Metasomatized and Regional Mantles	Azores	Metasomatized and Regional Mantles
Ol	0.604	0.52	0.08	−0.1
Opx	0.189	0.38	−0.19	0.35
Cpx	0.15	0.1	0.81	0.75
Gt	0.057	0	0.3	

[a]*Salters and Stracke* [2004].

component" [*Turner et al.*, 1997]. The observed differences in major and trace elements between the Azores MORB (KP-2 and -3) and isotopically similar Azores island basalts largely reflect lower extents of melting in the islands (2%–5%) relative to the MORB (10%–15%) caused by the thick lithosphere beneath the islands [*Beier et al.*, 2010; *Turner et al.*, 1997; *White et al.*, 1979]. An Azores mantle source composition was calculated by *Gier* [2005] using a representative Azores platform sample (AII0127-1-R064) with high-quality ICP-MS trace element data. Given that KP-2 and -3 lavas can be considered to represent "plume" material, we will use this source in our modeling (composition given in Table 3).

5.1.1. The Mechanism of Low-F Melt Addition

[35] Two mechanisms of low-F melt addition must be considered. The first is mixing the low-F Azores melt directly with transitional group melts from each segment. This scenario is ruled out because enriched

samples have higher Al_2O_3 contents than transitional samples (see Figure 2b). Melts with garnet in the residue are characteristically low in Al_2O_3 [e.g., *Walter*, 1998], so the proposed low-F melt with garnet in the residue (required by the very low HREE abundances of the enriched samples), would have low Al_2O_3. Mixing a low-Al_2O_3 low-F melt with transitional melts would not create the higher Al_2O_3 contents of the enriched samples. In a recent study of the Azores islands, *Beier et al.* [2008] call for such low-F (1%–2%) melts in the garnet field to generate Sao Miguel (Azores) lavas. The estimated primitive Al_2O_3 contents of these magmas (10.8%) are lower than those of other Azores islands due to increased amounts of residual garnet.

[36] The second alternative is to add the low-F melt to a depleted mantle source, creating a mixed source that is subsequently melted. Low extents of mantle melting with garnet in the residue generate melts with strongly enriched highly incompatible trace element abundances and very low HREE contents. Adding even a small amount (<3%) of this low-F melt to a depleted source is enough to dominate its trace element signature (e.g., steeply sloping REE pattern). So this mixed source, upon being melted, will generate melts with trace element characteristics that show evidence of residual garnet even if none is present during the second melt stage. This is consistent with the high Al_2O_3 contents of the enriched lavas, which preclude garnet in the source during the second melting event. So the proposed model is two stage: first a low-F melt of a garnet-bearing Azores mantle source is generated. This melt is then added to a depleted mantle, creating a mixed source that is later melted without garnet in the residue. This model reconciles the seeming contradiction of a "garnet signature" in the trace elements and a "garnet-free signature" in the major elements.

[37] It is important to be clear about the phrase "depleted mantle source" used in this context. For example, extraction of a 2% mantle melt has very little effect on the major element composition of the residue, but can drastically deplete the incompatible element contents. For an incompatible element with a D of 0.001 (typical for Rb, Ba, Th, U), 2% melting can lead to 95% depletion of the residue, while if the melt contains 15% Al_2O_3 and the source 4% Al_2O_3, Al_2O_3 is very modestly diminished by less than 10%. And in an exactly analogous way, addition of this low-F melt to another source can greatly enrich the highly incompatible elements and have negligible effect on the major elements. While many now consider "enriched" and "depleted" to refer to an eclogite vein on the one hand, and a depleted harzburgite on the other, this is not the way we are using the terms. For the region under study, and indeed for much of the mantle heterogeneity signal, we (and others [e.g., *Donnelly et al.*, 2004; *Cooper et al.*, 2004; *Schilling et al.*, 1980]) suggest that movement of low-degree melts is central. This movement can cause drastic changes in trace element compositions while preserving a mantle lherzolite. "Depleted" in this context refers largely to incompatible elements, not major elements. Below we argue for less than 5% melt removal to create our depleted mantle source, significantly depleting trace elements while only modestly depleting major elements.

[38] To further develop the model, we turn to geophysical constraints. *Yang et al.* [2006], in a seismic tomography study near the Azores, show evidence that plume material upwelling near the island of Terceira is deflected to the southwest (the direction of regional upper mantle shear flow) toward the islands of Pico, Faial and Sao Jorge. They postulate that plume material then feeds perpendicular to the ridge system (to segments KP-2 and -3) along a sloping rheological boundary layer. Their tomographic model supports many previous geochemical and bathymetric studies showing extensive Azores plume influence south of the MAR and little influence to the north [e.g., *Schilling*, 1975; *White and Schilling*, 1978; *Goslin and Triatnord Sci*, 1999]. *Donnelly et al.* [2004] proposed that low-F partial melting that metasomatizes the surrounding mantle could occur in the "margins of plumes." Given these previous studies, we propose that low-F melting in the garnet field is taking place in the southwestern margin of the Azores plume. These melts then get injected into surrounding depleted lithospheric mantle, creating a metasomatized source that flows southwestward, eventually melting to form the enriched samples seen at Menez Gwen and Lucky Strike.

5.1.2. Major Element Systematics

[39] The proposed two-stage process is consistent with the major elements. Recall that low FeO, high K_2O and low SiO_2 distinguish the enriched samples in major element diagrams. It is difficult to generate parental magmas with simultaneously low FeO and low SiO_2, as both are sensitive to pressure of melting and have opposite behaviors, i.e., high-pressure melts are low-SiO_2 and high-FeO [e.g., *Jaques and Green*, 1980]. Melting a mantle with a higher Mg# lowers FeO contents [*Langmuir and Hanson*, 1980], but this effect is not pronounced enough to generate a suitable parental magma for the enriched magmas. Moreover, a more refractory

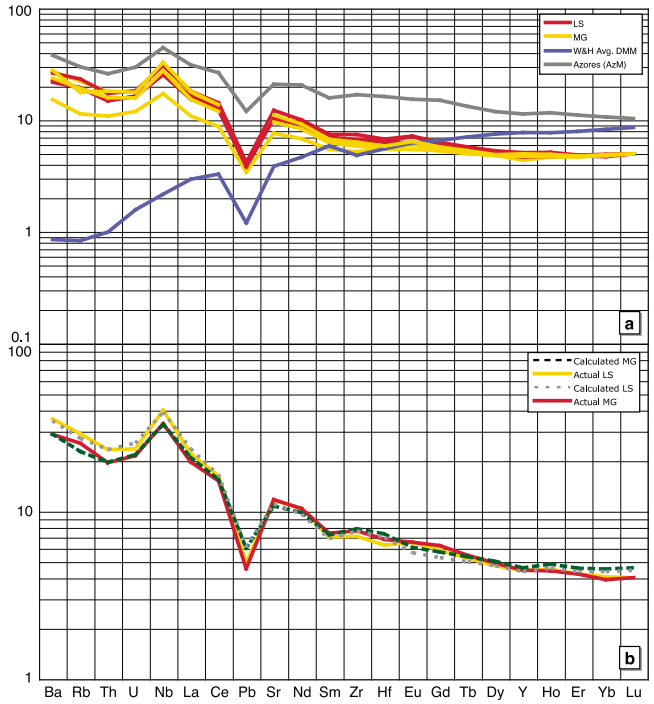

Figure 9. (a) Trace element patterns of the inverted metasomatized sources of seven primitive enriched samples from Menez Gwen and Lucky Strike, with the Azores source and the average DM from *Workman and Hart* [2005] for comparison. The nearly constant HREE in the metasomatized sources reflect the depleted source composition, whereas the large variability in the highly incompatible elements reflects the variable low-F addition. (b) Trace element patterns of representative enriched samples from Menez Gwen and Lucky Strike ("actual") compared to our best-fit model output ("calculated").

mantle would not likely melt at deep enough pressures to create low enough SiO_2, and it certainly would not have high enough K_2O or TiO_2 contents. The addition of low-F melts to a moderately refractory source (Mg #91), however, resolves this problem by significantly increasing the concentration of water and alkalis in the source. This increase in water and alkalis acts to (1) increase the mantle olivine K_d's, lowering the FeO in the melts [*Roeder*, 1974], (2) increase the K_2O contents to levels that are consistent with the enriched magmas at Lucky Strike and Menez Gwen, (3) depress the solidus so that melting can take place at higher pressures, compatible with the observed low SiO_2.

[40] In our major element model we calculate a mantle source composition and the extent(s) of melting required to generate parental magmas for the enriched samples. We estimated parental melt compositions by taking the seven most primitive enriched lavas (MgO > 8.2 wt.%) and adding incremental equilibrium olivine until the liquids were in equilibrium with Mg#91 olivine (moderately refractory mantle). We then calculated a mantle source by fixing its Mg# to 91 and optimizing the concentrations of major element oxides (allowing them to vary within a reasonable range) until appropriate parental melt(s) could be generated using the parameterization of *Langmuir et al.* [1992]. We find that pooled fractional melts with an integrated F of 6.5%–7.5% generate suitable parental melts for the enriched basalts at Lucky Strike and Menez Gwen (see Figure 2; two parental melts representing 6.5% and 7.5% melting are shown. Note that the parameterization of *Langmuir et al.* [1992] does not include Al_2O_3 or SiO_2, which is why no parental magmas are shown in Figures 2b and 2e). The composition of the source is given in Table 3 ("Metasomatized Mantle"). Note that our estimates of K_2O in this source agree with the amount of low-F melt added to the source (2%–2.6%) indicated by the trace element modeling detailed below.

[41] The fairly low (6.5%–7.5%) melting extent is reasonable considering the moderately refractory mantle source which likely limits melt productivity. An important question, however, is why the Al_2O_3 contents of enriched samples are higher than transitional samples if they are melts from a moderately refractory mantle. While we do not constrain Al_2O_3 in our melting model, based on the observed rela-

tionship between MgO and Al_2O_3 in mantle peridotites [*McDonough and Sun*, 1995 and data from GeoROC], we estimate that our mantle source has ~2.8% Al_2O_3. Adding ~2.6% of the low-F component (as suggested by the trace element modeling below) with ~10.8% Al_2O_3 (the Al_2O_3 contents of Sao Miguel low-F melts in the garnet field) brings the source to 3.1% Al_2O_3. This is lower than bulk DM estimates (4% Al_2O_3; [*Workman and Hart*, 2005]), but still much higher than harzburgites with Al_2O_3 contents typically <1%. The lower extents of melting (6.5%–7.5%) relative to normal MORB without garnet in the residue could then lead to higher Al_2O_3 enriched lavas, as Al_2O_3 tends to increase as extent of melting decreases.

5.1.3. Trace Element Modeling

[42] Incompatible trace element ratios and concentrations further refine the model by constraining the extent of melting of the low-F melt and the relative amount that must be added to the depleted source to generate appropriate metasomatized sources. Full details of the trace element modeling are provided in the auxiliary material; here we outline the concepts. A primary magma can be inverted for the trace element composition of its mantle source if F is known. We calculated primary incompatible trace element compositions of the seven enriched lavas from Menez Gwen and Lucky Strike by applying a dilution factor based on how much olivine was added to be in equilibrium with Mg#91 mantle (following the major element modeling above). We then inverted these primary magmas using a nonmodal batch melting equation and the constraints on F from the major element modeling to estimate the trace element composition of the metasomatized sources (see average "metasomatized" source composition, source mineralogy, D values and melting reactions in Table 3; the seven individual sources are provided in Table S5). The metasomatized sources are shown in Figure 9.

[43] The modeling assumes that the metasomatized sources consist of a single depleted source with variable amounts of low-F addition. This is reasonable given that the concentrations of HREE, elements largely unaffected by the low-F addition, are nearly constant in the enriched lavas (see Figure 3). We therefore use the HREE contents of the metasomatized sources to estimate the composition of the depleted mantle prior to the low-F addition. The HREE contents of the inverted sources (e.g., 0.034 ppm Lu) are lower than published values for depleted MORB mantle [e.g., *Workman and Hart*, 2005; *Salters and Stracke*, 2004], thus requiring a slightly more depleted "depleted source." This is not surprising given the moderately refractory source required to reconcile the low FeO contents of the enriched lavas. We calculated the composition of this depleted source (pre–low F addition) by extracting a 4.7% batch melt from the average MORB mantle reported in *Workman and Hart* [2005] so that the HREE contents matched the contents of the inverted sources. The source composition is given in Table 3 ("Mantle Source 1"). As noted above, this level of melt removal is enough to significantly deplete the trace elements with more moderate effects on major elements.

[44] We then minimized differences between the inverted sources and a source created by mixing low-F Azores melt with our Mantle Source 1, including absolute concentrations and key trace element ratios (e.g., La/Sm, Ba/La, Zr/Nb). We also minimized differences between subsequent batch melts of our mixed sources and the primary enriched lava compositions. We allowed three parameters to vary: (1) the F of the low-F of Azores mantle; (2) the quantity of that low-F added to Mantle Source 1; (3) the F of the metasomatized source. The nonmodal batch melting of the Azores source (the low-F event) took place with garnet in the source; the melting reactions and mineral modes are given in Table 3. Note that 5.7% garnet in our source is consistent with the ~4%–10% range of garnet in the source of Azores islands estimated by *Bourdon et al.* [2005].

[45] The fit was performed for each of the seven samples, and the results of the optimization can be found in Table S5. The metasomatized sources can be fit by this model with an average low-F of the Azores source of 3.8% (range 2.9%–4.8%) and an average addition of 2.2% (range 1.9%–2.6%) of that low-F to Mantle Source 1. Subsequent batch melting of these metasomatized sources between 6% and 7.7% (average of 7.2%) without garnet in the source beneath the ridge segments produces lavas equivalent to the observed enriched lavas. Shown in Figure 9b are trace element patterns of representative enriched lavas from Lucky Strike and Menez Gwen and the corresponding "best-fit" model melts. Also see Figure 4 for the compositional field spanned by the low-F melts.

5.1.4. Isotope Systematics

[46] Our model also accounts well for the isotopic data (Figure 5). The low concentrations of incompatible elements in our depleted source enable even

a small quantity of low-F addition to strongly influence the isotopic ratio of the metasomatized source. For example, of the metasomatized source Pb concentrations (average of 0.75 ppm), 95% of this Pb comes from the low-F melt addition. A melt of this source will then have isotopic ratios very similar to (but still lower than) Azores lavas. The low-F addition also reconciles another peculiar feature exhibited by the enriched Lucky Strike samples: they are more similar to the Azores lavas in Pb isotopes than they are in Sr isotopes. This again relates to the extent of depletion of the depleted source, and the amount that the low-F contributes to the overall trace element budget. The low-F (with Azores isotopic signature) contributes 95% of the Pb but only 90% of the Sr to the depleted source. As such, the low-F melts affect the source slightly more in Pb than in Sr, explaining why the enriched Lucky Strike samples nearly match the Azores in Pb isotopic ratios but are not as close in Sr isotopic ratios.

5.2. Origin of the Transitional Samples

5.2.1. Major Element Systematics

[47] The major element characteristics of the transitional basalts from Menez Gwen and Lucky Strike are similar enough to be considered here as one group. The differences in their $Si_{8.0}$ and $K_{8.0}$ are not large enough to affect our major element modeling, though they are consistent with a slightly more enriched source and deeper onset of melting moving northward toward the Azores. We estimated appropriate parental melt compositions for the transitional lavas by taking four of the most primitive samples (MgO > 8.9 wt.%) and adding incremental equilibrium olivine until the liquids were in equilibrium with Mg#89 olivine. Note that Mg#89 was used instead of Mg#91 because, as noted above, the average Mg# of transitional lavas is much lower than that of enriched lavas. Next, we estimated a mantle source by fixing its Mg# equal to 89 and optimizing the concentrations of the major element oxides until appropriate parental melt(s) could be generated using the parameterization of *Langmuir et al.* [1992]. Reasonable parental melts for the transitional basalts at Lucky Strike and Menez Gwen can be generated by pooling fractional melts with an integrated F of 7.2%–8.7% (see Figure 2, parental melts are shown representing 7.2% and 8.7% melting; Mantle Source 2 given in Table 3). Our major element modeling of one mantle source with variable F is an approximation, as obvious evidence in trace element and isotopic ratios exists for source heterogeneity between Menez Gwen and Lucky Strike. This source variation, however, seems to have minimal effects on most major elements.

5.2.2. Trace Element Systematics

[48] Clear differences in the trace element concentrations and isotopic ratios of transitional samples from Menez Gwen and Lucky Strike imply that their mantle sources contain different proportions of Azores mantle. We can use trace elements to estimate a "regional" mantle source (mixture of depleted mantle and Azores mantle) for Lucky Strike and Menez Gwen transitional samples. We first approximate a regional gradient by mixing in 10% increments the DM from *Salters and Stracke* [2004] with the Azores source (AzM) given in Table 3. We then melt this range of compositions 5% and 12% (see mineral proportions for "regional mantles" in Table 3) to generate a spectrum of regional melts to compare with our transitional samples from Menez Gwen and Lucky Strike (see Figures 4, 5, and 6 for regional gradient). We simplify our regional gradient modeling by assuming no garnet in the source, as neither the Menez Gwen nor the Lucky Strike transitional samples show evidence of a garnet-bearing source (see trace element patterns, Figure 3).

[49] These "regional melts" can then be used to estimate the regional mantle sources of transitional Menez Gwen and Lucky Strike lavas. This is straightforward for the transitional Menez Gwen basalts because they fall near the calculated regional gradient (Figure 4b). Their regional mantle source contains between 25% and 55% AzM. Much of the trace element variability seen in the transitional Menez Gwen samples, therefore, can be attributed to source variation. The transitional Lucky Strike samples deviate from the regional gradient toward higher highly incompatible element ratios, so estimating their regional mantle source(s) is not so straightforward. We approximate their regional mantle composition by fitting a curve to the transitional Lucky Strike lavas in the Sm/La versus Ba/La plot; the intersection of this curve with the modeled regional gradient is taken as an estimate of the Lucky Strike regional mantle. An appropriate regional mantle contains 10%–15% AzM and 90%–85% DM. For simplicity, the trace element modeling below (and shown in Figure 4) assumes 15% AzM in the Lucky Strike regional mantle source.

[50] The relative enrichment of transitional Lucky Strike samples compared to the calculated regional gradient requires explanation. Note that their trend is

between the regional mantle melts and the field for both the enriched samples and the low-F of AzM (see Figure 4b). This apparent mixing curve could be produced either through the variable addition of enriched melts to regional melts, through the addition of a low-F melt itself to either the regional mantle source or melts, or through mixing between the enriched (metasomatized) and regional mantle sources. As mentioned above, however, the similarities between the enriched Menez Gwen and Lucky Strike samples imply that the low-F process giving rise to these samples is not segment specific. We argue that the low-F of AzM is being generated at the edge of the Azores plume and not beneath individual ridge segments. This leads us to the conclusion that the transitional Lucky Strike samples reflect mixing between either enriched and regional melts or enriched (metasomatized) and regional mantle sources, rather than direct contribution from the Azores plume low-F melt. Mixing with the enriched melt (or metasomatized mantle source) imparts a bit of the low-F signature to the transitional Lucky Strike melts, which explains their anomalously high Ba/La compared to Menez Gwen transitional lavas (see Figures 4b and 7). We cannot distinguish between the two possibilities (source versus melt mixing) for generating Lucky Strike transitional lavas, but to demonstrate the concept we model melt mixing. We find that mixing a regional melt with between 10% and 60% of a representative enriched melt (AII0127-2-R116-002) accounts well for the transitional Lucky Strike samples.

5.2.3. Isotope Systematics

[51] We now consider the models for generating Lucky Strike and Menez Gwen transitional samples in light of isotopic constraints. The more enriched isotopic ratios of Menez Gwen samples compared to those of Lucky Strike are consistent with a larger proportion of AzM in their mantle source. In detail, a gap can be seen between transitional Lucky Strike and Menez Gwen samples in the $^{208}Pb/^{204}Pb$ versus $^{206}Pb/^{204}Pb$ diagram (Figure 5a). This gap agrees with our estimated difference between the amount of AzM in the regional mantle at Lucky Strike (~10%–15%) and at Menez Gwen (~25%–55%). The Pico transform fault between Menez Gwen and Lucky Strike may be somewhat limiting to the southern flow of AzM. With regard to Menez Gwen specifically, there are only three transitional samples with both isotopic and ICP-MS trace element data. It is thus difficult to test whether the samples that we propose have more AzM in their source using trace elements are more enriched isotopically.

[52] At Lucky Strike, our model must account for the clear isotopic variation within the transitional samples. Basalts with more enriched melt contribution indicated by trace elements should be more enriched isotopically, and this indeed turns out to be the case (Figure 5). Our calculated mixing curves between a regional mantle with 10%–15% AzM and the enriched samples cover the range of isotopic variation in the transitional samples (Figures 5 and 6). Also importantly, the absolute proportions of enriched melt added to the regional melt inferred from trace elements remain appropriate for the isotopic data. The isotopic composition of DM and AzM are given in Table 3.

5.3. Constraints on Crustal Accretion Processes

[53] We now consider the implications of our data set for the melt delivery styles along this portion of the MAR. Here our focus will be on Lucky Strike, as there are far more geophysical studies that, together with our new geochemical data, provide valuable constraints on the nature of the melt delivery process. The key observations from geophysical and seismic studies are: (1) the presence of a magma chamber 3.4 km beneath the central volcanic region, extending ~6 km along axis [*Singh et al.*, 2006], (2) the systematic thickening of the lithosphere from ~6.5 km at the segment center to 10 km at the segment edges [*Dusunur et al.*, 2009; *Cannat*, 1996], and (3) evidence for a recent dike intrusion [*Dziak et al.*, 2004]. These three features, combined with the presence of a robust central volcano, all suggest a significant role of focused, central delivery of melts to the Lucky Strike segment with at least some lateral diking. This process is similar to the one proposed by *Singh et al.* [2006]. Indeed, *Dusunur et al.* [2009] argue that the lithospheric geometry implied by their seismic observations promotes overall flow "upslope" to the center of the segment, further supporting the idea of focused melt delivery at Lucky Strike. Clear evidence exists for a component of "central supply," but it does not preclude that modest amounts of magma are emplaced throughout the segment rather than exclusively at the segment center.

[54] The stratigraphy of lava flows at Lucky Strike implies temporal geochemical variation. According to *Langmuir et al.* [1997], the highly vesicular, enriched lavas that comprise the main flanks of the central volcano are moderately altered and underlie the eruptions of fresh, glassy transitional lavas in the summit basin that appear to have erupted recently. This provides clear evidence that: (1) the enriched

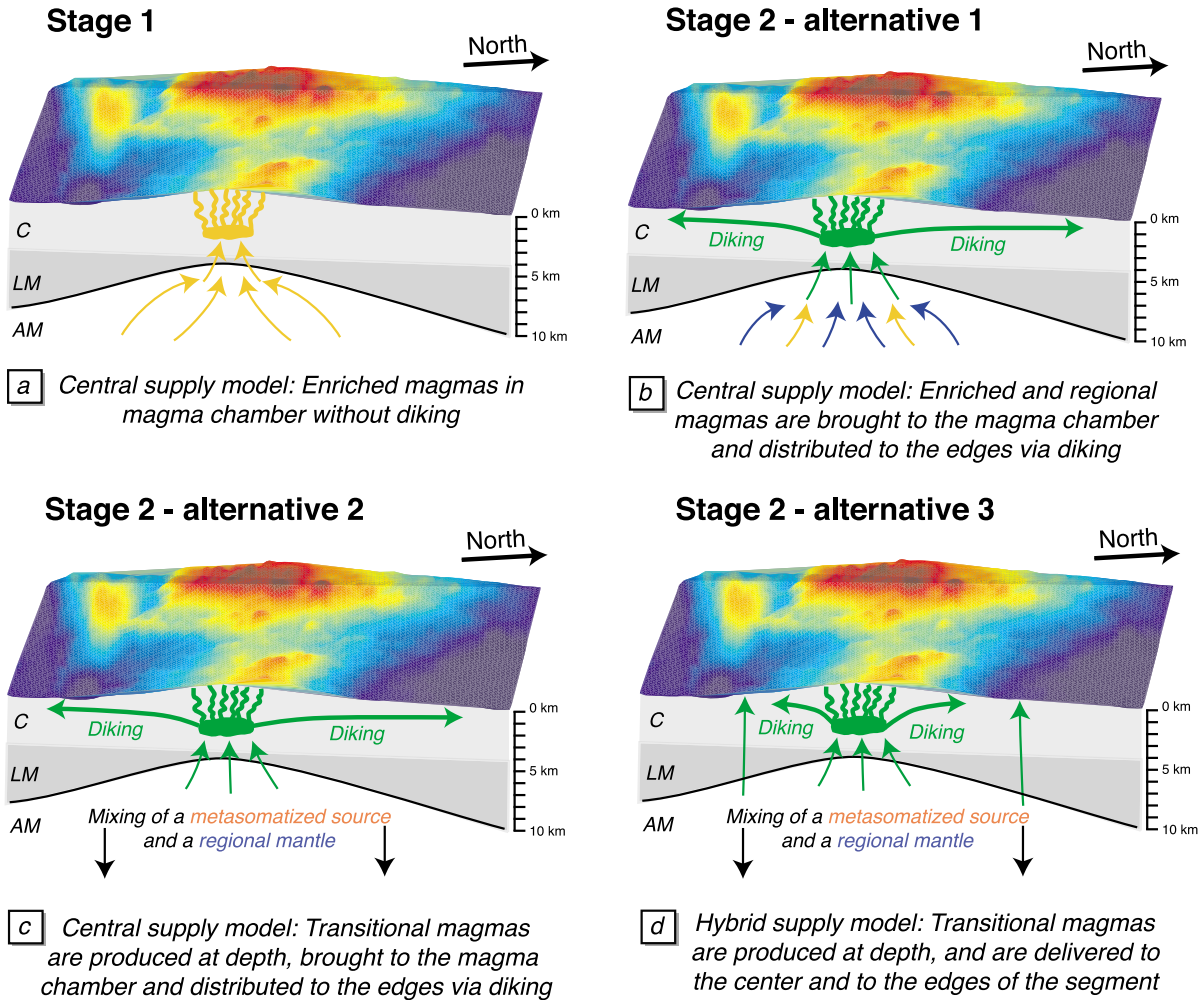

Figure 10. Cartoons illustrating possible models to explain the data at Lucky Strike. To explain the enrichment relative to the regional gradient, mixing of the enriched melts or source with the regional gradient melts or source is proposed. This could occur either as melt mixing at shallow levels, or through source mixing at depth. During Stage 1, enriched lavas are erupted at the center of the segment, to account for the enriched samples that make up much of the older edifice of Lucky Strike seamount. The more recent magmatism has three options. Alternative 1 shows mixing of melts at shallow levels, delivery to the segment center, and distribution through diking. Blue and yellow arrows represent regional and enriched melts, respectively. Alternative 2 illustrates source mixing at depth followed by central supply. Alternative 3 is source mixing at depth with most magma delivered to the segment center, but some to the segment ends, the "hybrid supply" model. C refers to crust, LM to lithospheric mantle, and AM to asthenospheric mantle.

lavas are older magmas and (2) recent lavas (and likely the magma chamber beneath) are made up of transitional magma. This evidence for discrete eruptions is consistent with the observations of *Dziak et al.* [2004], who suggest that volcanic activity at Lucky Strike may be caused by highly focused magma bodies that create "sporadic intrusions" into the shallow ocean crust.

[55] The geologic evidence implies that the coexistence of transitional and enriched groups at the segment center reflects temporal variability, and that the magma chamber must be short-lived. The enriched melts represent an earlier, distinct volcanic eruption at the center of the segment. The absence of enriched lavas at segment edges suggests that if a magma chamber were involved, there was no dike propagation toward the segment edges. Then, more recently, regional melts have been variably mixed with enriched melts within the melting regime to produce the transitional lavas. A significant proportion of the transitional melts must be focused toward the segment center, as they are found in the current central lava lake and are likely in the magma chamber below [*Singh et al.*, 2006].

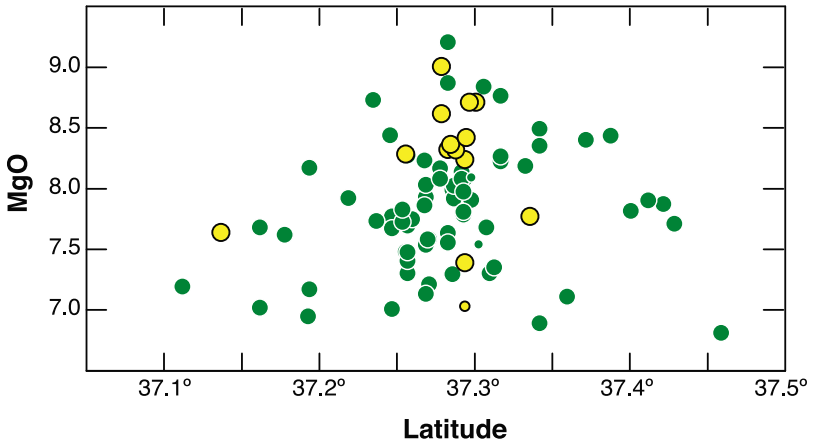

Figure 11. MgO versus latitude for samples from the Lucky Strike segment. There is a nearly symmetrical decrease in MgO content away from segment center, consistent with more pronounced cooling and crystallization in magmas at the edges of the segment.

[56] Two possibilities remain for the generation of the transitional ocean crust at the most distal segment edges. One possibility is that lateral diking of these variably mixed transitional melts from the magma chamber creates the crust at the segment edges (see Figures 10b and 10c). An alternative idea is that melt travels vertically from the edges of the melting regime through the thicker lithosphere to erupt on the ocean floor (see Figure 10d). Both lateral diking (central supply) and vertical transport through the lithosphere (multiple supply) could account for why the MgO contents decrease in the transitional samples toward the edges of the segment (see Figure 11). Cooling and fractionation (decreasing the MgO) of the lavas could occur either through extensive vertical travel through the thicker lithosphere at segment edges or through long lateral travel away from the segment center.

[57] There are issues with both possibilities. For the pure central supply model, a question is whether or not diking for 30 km (from segment center to edge) is reasonable. Diking may instead be confined to the central ±15 km of segment. For the "hybrid supply" model which combines melt focusing to the center with vertical transport of melts to the edges, melt focusing cannot be as efficient as it was for the enriched lavas, where all magma was centrally injected. Exactly what would cause melt focusing to be more or less efficient through time is not clear.

[58] A test of these ideas is whether there is a within-segment gradient in chemical composition. Given all the complexities involving enriched and transitional magmas, temporal variability and two distinct processes of mixing in Azores components, such a test is conceptually simple, but in practice complex to interpret. Isotopes are strongly influenced by the mixing systematics, as are highly incompatible trace elements. It is perhaps in the moderately incompatible elements, less influenced by the low-F melts but still influenced by the regional gradient, that within-segment variations could be observed. There does appear to be a gradual increase northward in Zr/Y and Sm/Yb within Lucky Strike and Menez Gwen (Figures 7c and 7d), and this variation would be consistent with a within-segment gradient that could be produced only by multiple supply.

[59] We are then left with a conflicting assessment of segmentation models. In support of central supply is the step function in isotopes, the existence of maximum chemical variability in the center of the segment and the robust central volcano. These results could suggest that diverse magmas appear at the center of the segment, and are homogenized and cooled as they propagate to the segment ends. In this case, however, why would not all the magmas have propagated to the segment ends, producing equal variability at all segment positions? Multiple supply also has support and hurdles to overcome. The gradients in moderately incompatible element ratios suggest within-segment variations. It would be more conclusive, however, if the gradients were present in all incompatible element and isotope ratios. Multiple supply would also require melting and transport models that would lead to more variable magmas delivered to the segment center, and a physical mechanism for preferential delivery of enriched magmas to segment centers. Ultimately these models would be best tested by more complete sampling of the segment ends, capture of an eruption in process that shows the extent of diking, or possibly an

eruption at a segment end not associated with seismicity and volcanism at the segment center. At this point the data seem to suggest a hybrid supply model where aspects of both central and multiple supply contribute to the segment scale variations.

6. Conclusions

[60] The main results of our study can be summarized as follows:

[61] 1. The regional gradient south of the Azores is complex in detail. Mean compositions of transitional samples are more enriched in isotopic ratios and most incompatible trace elements at Menez Gwen than Lucky Strike, consistent with the gradient. However, enriched samples, with even higher incompatible element ratios than the Azores platform, occur near the center of both segments.

[62] 2. There is clear evidence for low-F melt involvement in the generation of enriched samples from Menez Gwen and Lucky Strike not seen in samples from the Azores platform. The low-F of Azores mantle acts to metasomatize a depleted mantle source prior to the main melting event.

[63] 3. There is an enhanced low-F signature in the transitional lavas at Lucky Strike. Transitional basalts from Lucky Strike do not lie on the regional gradient and are offset to higher highly incompatible trace element ratios; they are formed through variable mixing of the regional melts (or mantle source) with the enriched melts (or mantle source).

[64] 4. The geochemical and geophysical evidence are not conclusive with respect to the multiple supply and central supply models. A "hybrid supply" model, incorporating aspects of both multiple and central supply, is most consistent with all of the data. The generality of this model remains to be determined by studies of many segments with diverse geological characteristics.

Acknowledgments

[65] We warmly thank E. L. Evans for help with Matlab to create the cartoon in Figure 10. Thanks also to Zhongxing Chen at Harvard University for his support with SN-ICP-MS analyses. The manuscript greatly benefited from thoughtful reviews by V. Salters and M. Perfit.

References

Agranier, A., J. Blichert-Toft, D. Graham, V. Debaille, P. Schiano, and F. Albarede (2005), The spectra of isotopic heterogeneities along the Mid-Atlantic Ridge, *Earth Planet. Sci. Lett.*, *238*(1–2), 96–109, doi:10.1016/j.epsl.2005.07.011.

Beier, C., A. Stracke, and K. M. Haase (2007), The peculiar geochemical signatures of Sao Miguel (Azores) lavas: Metasomatised or recycled mantle sources?, *Earth Planet. Sci. Lett.*, *259*(1–2), 186–199, doi:10.1016/j.epsl.2007.04.038.

Beier, C., K. M. Haase, W. Abouchami, M. S. Krienitz, and F. Hauff (2008), Magma genesis by rifting of oceanic lithosphere above anomalous mantle: Terceira Rift, Azores, *Geochem. Geophys. Geosyst.*, *9*, Q12013, doi:10.1029/2008GC002112.

Beier, C., S. Turner, T. Plank, and W. White (2010), A preliminary assessment of the symmetry of source composition and melting dynamics across the Azores plume, *Geochem. Geophys. Geosyst.*, *11*, Q02004, doi:10.1029/2009GC002833.

Bender, J. F., C. H. Langmuir, and G. N. Hanson (1984), Petrogenesis of basalt glasses from the Tamayo Region, East Pacific Rise, *J. Petrol.*, *25*(1), 213–254.

Bourdon, B., S. P. Turner, and N. M. Ribe (2005), Partial melting and upwelling rates beneath the Azores from a U-series isotope perspective, *Earth Planet. Sci. Lett.*, *239*(1–2), 42–56, doi:10.1016/j.epsl.2005.08.008.

Bryan, W. B. (1979), Regional variation and petrogenesis of basalt glasses from the FAMOUS area, Mid-Atlantic Ridge, *J. Petrol.*, *20*(2), 293–325.

Bryan, W. B., and J. G. Moore (1977), Compositional variations of young basalts in the Mid-Atlantic Ridge rift valley near lat 36°49′N, *Geol. Soc. Am. Bull.*, *88*, 556–570.

Cannat, M. (1996), How thick is the magmatic crust at slow spreading oceanic ridges?, *J. Geophys. Res.*, *101*(B2), 2847–2857, doi:10.1029/95JB03116.

Cannat, M., et al. (1999), Mid-Atlantic Ridge-Azores hotspot interactions: Along-axis migration of a hotspot-derived event of enhanced magmatism 10 to 3 Ma ago, *Earth Planet. Sci. Lett.*, *173*(3), 257–269, doi:10.1016/S0012-821X(99)00234-4.

Chauvel, C., and J. Blichert-Toft (2001), A hafnium isotope and trace element perspective on melting of the depleted mantle, *Earth Planet. Sci. Lett.*, *190*(3–4), 137–151, doi:10.1016/S0012-821X(01)00379-X.

Combier, V. (2007), Mid-ocean ridge processes: Insights from 3D reflection seismics at the 9°N OSC on the East Pacific Rise, and the Lucky Strike Volcano on the Mid-Atlantic Ridge, Ph.D. thesis, Inst. de Phys. du Globe de Paris, Paris.

Cooper, K. M., J. M. Eller, P. D. Asimow, and C. H. Langmuir (2004), Oxygen isotope evidence for the origin of enriched mantle beneath the Mid-Atlantic ridge, *Earth Planet. Sci. Lett.*, *220*(3–4), 297–316, doi:10.1016/S0012-821X(04)00058-5.

Curewitz, D., and J. A. Karson (1998), Geological consequences of dike intrusion at mid-ocean ridge spreading centers, in *Faulting and Magmatism at Mid-Ocean Ridges*, *Geophys. Monogr. Ser.*, vol. 106, edited by W. R. Buck et al., pp. 117–136, AGU, Washington D. C.

Detrick, R., H. Needham, and V. Renard (1995), Gravity anomalies and crustal thickness variations along the Mid-Atlantic Ridge between 33°N and 40°N, *J. Geophys. Res.*, *100*(B3), 3767–3787, doi:10.1029/94JB02649.

Donnelly, K. E., S. L. Goldstein, C. H. Langmuir, and M. Spiegelman (2004), Origin of enriched ocean ridge basalts and implications for mantle dynamics, *Earth Planet. Sci. Lett.*, *226*(3–4), 347–366, doi:10.1016/j.epsl.2004.07.019.

Dosso, L., H. Bougault, C. Langmuir, C. Bollinger, O. Bonnier, and J. Etoubleau (1999), The age and distribution of mantle

heterogeneity along the Mid-Atlantic Ridge (31–41°N), *Earth Planet. Sci. Lett.*, *170*(3), 269–286, doi:10.1016/S0012-821X(99)00109-0.

Dusunur, D., J. Escartín, V. Combier, T. Seher, W. Crawford, M. Cannat, S. C. Singh, L. M. Matias, and J. M. Miranda (2009), Seismological constraints on the thermal structure along the Lucky Strike segment (Mid-Atlantic Ridge) and interaction of tectonic and magmatic processes around the magma chamber, *Mar. Geophys. Res.*, *30*(2), 105–120, doi:10.1007/s11001-009-9071-3.

Dziak, R. P., D. K. Smith, D. R. Bohnenstiehl, C. G. Fox, D. Desbruyeres, H. Matsumoto, M. Tolstoy, and D. J. Fornari (2004), Evidence of a recent magma dike intrusion at the slow spreading Lucky Strike segment, Mid-Atlantic Ridge, *J. Geophys. Res.*, *109*, B12102, doi:10.1029/2004JB003141.

Embley, R. W., W. W. Chadwick, I. R. Jonasson, D. A. Butterfield, and E. T. Baker (1995), Initial results of the rapid response to the 1993 CoAxial event: Relationships between hydrothermal and volcanic processes, *Geophys. Res. Lett.*, *22*(2), 143–146, doi:10.1029/94GL02281.

Escartín, J., M. Cannat, G. Pouliquen, A. Rabain, and J. Lin (2001), Crustal thickness of V-shaped ridges south of the Azores: Interaction of the Mid-Atlantic Ridge (36°–39°N) and the Azores hot spot, *J. Geophys. Res.*, *106*(B10), 21,719–21,735, doi:10.1029/2001JB000224.

Fouquet, Y., H. Ondréas, J.-L. Charlou, J.-P. Donval, J. Radford-Knoery, I. Coasta, N. Lourenco, and M. K. Tivey (1995), Atlantic lava lakes and hot vents, *Nature*, *377*, 201, doi:10.1038/377201a0.

Fox, C. G., W. E. Radford, R. P. Dziak, T. K. Lau, H. Matsumoto, and A. E. Schreiner (1995), Acoustic detection of a sea-floor spreading episode on the Juan-de-Fuca Ridge using military hydrophone arrays, *Geophys. Res. Lett.*, *22*(2), 131–134, doi:10.1029/94GL02059.

Frey, F. A., N. Walker, D. Stakes, S. R. Hart, and R. Nielson (1993), Geochemical characteristics of basalt glasses from the AMAR and FAMOUS axial valleys, Mid-Atlantic Ridge (36°–37°N): Petrogenic implications, *Earth Planet. Sci. Lett.*, *115*, 117–136, doi:10.1016/0012-821X(93)90217-W.

Gier, E. J. (2005), The geological implications of the basalts and sediments of the Lucky Strike Segment, 195 pp., Columbia Univ., New York.

Goslin, J., and P. Triatnord Sci (1999), Extent of Azores plume influence on the Mid-Atlantic Ridge north of the hotspot, *Geology*, *27*(11), 991–994, doi:10.1130/0091-7613(1999)027<0991:EOAPIO>2.3.CO;2.

Gudmundsson, A. (1998), Magma chambers modeled as cavities explain the formation of rift zone central volcanoes and their eruption and intrusion statistics, *J. Geophys. Res.*, *103*(B4), 7401–7412, doi:10.1029/97JB03747.

Hooft, E. E. E., R. S. Detrick, D. R. Toomey, J. A. Collins, and J. Lin (2000), Crustal thickness and structure along three contrasting spreading segments of the Mid-Atlantic Ridge, 33.5–35°N, *J. Geophys. Res.*, *105*(B4), 8205–8226, doi:10.1029/1999JB900442.

Ito, E., W. M. White, and C. Goepel (1987), The O, Sr, Nd and Pb isotope geochemistry of MORB, *Chem. Geol.*, *62*, 157–176, doi:10.1016/0009-2541(87)90083-0.

Jaques, A. L., and D. H. Green (1980), Anhydrous melting of peridotite at 0–15 kb pressure and genesis of tholeiitic basalts, *Contrib. Mineral. Petrol.*, *73*, 287–310, doi:10.1007/BF00381447.

Kuo, B.-Y., and D. W. Forsyth (1988), Gravity anomalies of the ridge-transform system in the South Atlantic between 31 and 34.5°S: Upwelling centers and variations in crustal thickness, *Mar. Geophys. Res.*, *10*, 205–232, doi:10.1007/BF00310065.

Langmuir, C. H., and G. Hanson (1980), An evaluation of major element heterogeneity in the mantle sources of basalts, *Philos. Trans. R. Soc. London A*, *297*, 383–407, doi:10.1098/rsta.1980.0223.

Langmuir, C. H., J. F. Bender, A. E. Bence, G. N. Hanson, and S. R. Taylor (1977), Petrogenesis of basalts from the FAMOUS Area: Mid-Alantic Ridge, *Earth Planet. Sci. Lett.*, *36*(1), 133–156, doi:10.1016/0012-821X(77)90194-7.

Langmuir, C. H., J. F. Bender, and R. Batiza (1986), Petrological and tectonic segmentation of the East Pacific Rise, 5°30′–14°30′ N, *Nature*, *322*(6078), 422–429, doi:10.1038/322422a0.

Langmuir, C. H., E. M. Klein, and T. Plank (1992), Petrological systematics of Mid-Ocean ridge basalts: Constraints on melt generation beneath ocean ridges, in *Mantle Flow and Melt Generation at Mid-Ocean Ridges*, *Geophys. Monogr. Ser.*, vol. 71, edited by J. Phipps Morgan, D. K. Blackman, and J. M. Sinton, pp. 183–280, AGU, Washington, D. C.

Langmuir, C. H., et al. (1997), Hydrothermal vents near a mantle hot spot: The Lucky Strike vent field at 37°N on the Mid-Atlantic Ridge, *Earth Planet. Sci. Lett.*, *148*, 69–91, doi:10.1016/S0012-821X(97)00027-7.

Lawson, K., R. C. Searle, J. A. Pearce, P. Browning, and P. Kempton (1996), Detailed volcanic geology of the MARNOK area, Mid-Atlantic Ridge north of Kane transform, in *Tectonic, Magmatic, Hydrothermal and Biological Segmentation of Mid-Ocean Ridges*, edited by C. J. MacLeod, P. Tyler, and C. L. Walker, *Geol. Soc. Spec. Publ.*, *102*, 61–102.

leRoex, A. P., A. J. Erlank, and H. D. Needham (1981), Geochemical and mineralogical evidence for the occurrence of at least three distinct magma types in the 'famous' region, *Contrib. Mineral. Petrol.*, *77*, 24–37, doi:10.1007/BF01161499.

Magde, L. S., and D. W. Sparks (1997), Three-dimensional mantle upwelling, melt generation, and melt migration beneath segment slow spreading ridges, *J. Geophys. Res.*, *102*(B9), 20,571–20,583, doi:10.1029/97JB01278.

Magde, L. S., A. H. Barclay, D. R. Toomey, R. S. Detrick, and J. A. Collins (2000), Crustal magma plumbing within a segment of the Mid-Atlantic Ridge, 35°N, *Earth Planet. Sci. Lett.*, *175*, 55–67, doi:10.1016/S0012-821X(99)00281-2.

McDonough, W. F., and S. Sun (1995), The composition of the Earth, *Chem. Geol.*, *120*, 223–253, doi:10.1016/0009-2541(94)00140-4.

Melson, W. G., T. O'Hearn, and E. Jarosewich (2002), A data brief on the Smithsonian Abyssal Volcanic Glass Data File, *Geochem. Geophys. Geosyst.*, *3*(4), 1023, doi:10.1029/2001GC000249.

Michael, P. J., R. L. Chase, and J. F. Allan (1989), Petrologic and geologic variations along the Southern Explorer Ridge, northeast Pacific Ocean, *J. Geophys. Res.*, *94*(B10), 13895–13918.

Moreira, M., and C. J. Allegre (2002), Rare gas systematics on Mid-Atlantic Ridge (37–40°N), *Earth Planet. Sci. Lett.*, *198*(3–4), 401–416, doi:10.1016/S0012-821X(02)00519-8.

Moreira, M., R. Doucelance, M. D. Kurz, B. Dupre, and C. J. Allegre (1999), Helium and lead isotope geochemistry of the Azores Archipelago, *Earth Planet. Sci. Lett.*, *169*(1–2), 189–205, doi:10.1016/S0012-821X(99)00071-0.

Morgan, J. P., and D. W. Forsyth (1988), Three-dimensional flow and temperature perturbations due to a transform offset: Effects on oceanic crustal and upper mantle structure, *J. Geophys. Res.*, *93*(B4), 2955–2966, doi:10.1029/JB093iB04p02955.

Natland, J. H., and W. G. Melson (1980), Composition of basaltic glasses from the east Pacific Rise and Siqueiros Fracture Zone near 9°N, *Initial Rep. Deep Sea Drill. Proj.*, *54*, 705–723.

Nishio, Y., S. Nakai, T. Ishii, and Y. Sano (2007), Isotope systematics of Li, Sr, Nd, and volatiles in Indian Ocean MORBs of the Rodrigues Triple Junction: Constraints on the origin of the DUPAL anomaly, *Geochim. Cosmochim. Acta*, *71*(3), 745–759, doi:10.1016/j.gca.2006.10.004.

Niu, Y. L., and R. Batiza (1994), Magmatic processes at a slow spreading ridge segment: 26°S Mid-Atlantic Ridge, *J. Geophys. Res.*, *99*(B10), 19,719–19,740, doi:10.1029/94JB01663.

Ondréas, H., Y. Fouquet, M. Voisset, and J. Radford-Knoery (1997), Detailed study of three contiguous segments of the Mid-Atlantic Ridge, south of the Azores (37°N to 38°30′ N), using acoustic imaging coupled with submersible observations, *Mar. Geophys. Res.*, *19*, 231–255, doi:10.1023/A:1004230708943.

Parfitt, E. A. (1991), The role of rift-zone storage in controlling the site and timing of eruptions and intrusions of Kilauea volcano, Hawaii, *J. Geophys. Res.*, *96*(B6), 10,101–10,112, doi:10.1029/89JB03559.

Parson, L., E. Gracia, D. Coller, C. German, and D. Needham (2000), Second order segmentation: The relationship between volcanism and tectonism at the MAR, 38°N–35°40′ N, *Earth Planet. Sci. Lett.*, *178*, 231–251, doi:10.1016/S0012-821X(00)00090-X.

Reynolds, J., and C. Langmuir (1997), Petrological systematics of the Mid-Atlantic Ridge south of Kane: Implications for ocean crust formation, *J. Geophys. Res.*, *102*(B7), 14,915–914,946, doi:10.1029/97JB00391.

Roeder, P. L. (1974), Activity of iron and olivine solubility in basaltic liquids, *Earth Planet. Sci. Lett.*, *23*(3), 397–410, doi:10.1016/0012-821X(74)90129-0.

Ryan, W. B. F., et al. (2009), Global Multi-Resolution Topography synthesis, *Geochem. Geophys. Geosyst.*, *10*, Q03014, doi:10.1029/2008GC002332.

Salters, V. J. M., and A. Stracke (2004), Composition of the depleted mantle, *Geochem. Geophys. Geosyst.*, *5*, Q05B07, doi:10.1029/2003GC000597.

Schilling, J. G. (1975), Azores mantle blob: Rare-Earth evidence, *Earth Planet. Sci. Lett.*, *25*(2), 103–115, doi:10.1016/0012-821X(75)90186-7.

Schilling, J. G., and H. Sigurdsson (1979), Thermal minima along the axis of the Mid-Atlantic ridge, *Nature*, *282*, 370–375, doi:10.1038/282370a0.

Schilling, J. G., M. B. Bergeron, and R. Evans (1980), Halogens in the mantle beneath the North Atlantic, *Philos. Trans. R. Soc. London A*, *297*(1431), 147–178, doi:10.1098/rsta.1980.0208.

Schilling, J. G., M. Zajac, R. Evans, T. Johnston, W. White, J. D. Devine, and R. Kingsley (1983), Petrologic and geochemical variations along the Mid-Atlantic Ridge from 29°N to 73°N, *Am. J. Sci.*, *283*(6), 510–586, doi:10.2475/ajs.283.6.510.

Schouten, H., K. D. Klitgord, and J. A. Whitehead (1985), Segmentation of mid-ocean ridges, *Nature*, *317*, 225–229, doi:10.1038/317225a0.

Seher, T., W. C. Crawford, S. C. Singh, and M. Cannat (2010), Seismic layer 2A variations in the Lucky Strike segment at the Mid-Atlantic Ridge from reflection measurements, *J. Geophys. Res.*, *115*, B07107, doi:10.1029/2009JB006783.

Sigurdsson, H. (1981), First-order major element variation in basalt glasses from the Mid-Atlantic Ridge: 29° N to 73° N, *J. Geophys. Res.*, *86*(B10), 9483–9502, doi:10.1029/JB086iB10p09483.

Singh, S. C., W. C. Crawford, H. Carton, T. Seher, V. Combier, M. Cannat, J. P. Canales, D. Dusunur, J. Escartín, and J. M. Miranda (2006), Discovery of a magma chamber and faults beneath a Mid-Atlantic Ridge hydrothermal field, *Nature*, *442*(7106), 1029–1032, doi:10.1038/nature05105.

Sinton, J. M., S. M. Smaglik, J. J. Mahoney, and K. C. Macdonald (1991), Magmatic processes at superfast spreading mid ocean ridges: Glass compositional variations along the East Pacific rise 13°– 23° S, *J. Geophys. Res.*, *96*(B4), 6133–6155, doi:10.1029/90JB02454.

Thompson, G., and W. G. Melson (1972), The petrology of oceanic crust across fracture zones in the Atlantic Ocean: Evidence of a new kind of sea-floor spreading, *J. Geol.*, *80*, 526–538, doi:10.1086/627779.

Todt, W., R. A. Cliff, A. Hanser, and A. W. Hofmann (1996), Evaluation of a ^{202}Pb–^{205}Pb double spike for high-precision lead isotope analysis, in *Earth Processes: Reading the Isotopic Code*, *Geophys. Monogr. Ser.*, edited by A. Basu and S. Hart, pp. 429–437, AGU, Washington, D. C.

Turner, S., C. Hawkesworth, N. Rogers, and P. King (1997), U-Th isotope disequilibria and ocean island basalt generation in the Azores, *Chem. Geol.*, *139*(1–4), 145–164, doi:10.1016/S0009-2541(97)00031-4.

Walter, M. J. (1998), Melting of garnet peridotite and the origin of komatiite and depleted lithosphere, *J. Petrol.*, *39*(1), 29–60, doi:10.1093/petrology/39.1.29.

White, W. M., and W. B. Bryan (1977), Sr-isotope, K, Rb, Cs, Sr, Ba, and rare earth geochemistry of basalts from the FAMOUS area, *Geol. Soc. Am. Bull*, *88*, 571–576, doi:10.1130/0016-7606(1977)88<571:SKRCSB>2.0.CO;2.

White, W. M., and J. G. Schilling (1978), The nature and origin of geochemical variation in Mid-Atlantic Ridge basalts from central North Atlantic, *Geochim. Cosmochim. Acta*, *42*, 1501–1516, doi:10.1016/0016-7037(78)90021-2.

White, W. M., M. D. M. Tapia, and J. G. Schilling (1979), Petrology and geochemistry of the Azores Islands, *Contrib. Mineral. Petrol.*, *69*(3), 201–213, doi:10.1007/BF00372322.

Widom, E., R. W. Carlson, J. B. Gill, and H. U. Schmincke (1997), Th-Sr-Nd-Pb isotope and trace element evidence for the origin of the Sao Miguel, Azores, enriched mantle source, *Chem. Geol.*, *140*(1–2), 49–68, doi:10.1016/S0009-2541(97)00041-7.

Workman, R. K., and S. B. Hart (2005), Major and trace element composition of the depleted MORB mantle (DMM), *Earth Planet. Sci. Lett.*, *231*, 53–72, doi:10.1016/j.epsl.2004.12.005.

Yang, T., Y. Shen, S. van der Lee, S. C. Solomon, and S. H. Hung (2006), Upper mantle structure beneath the Azores hotspot from finite-frequency seismic tomography, *Earth Planet. Sci. Lett.*, *250*(1–2), 11–26, doi:10.1016/j.epsl.2006.07.031.

Yi, W., A. N. Halliday, J. C. Alt, D. C. Lee, M. Rehkamper, M. O. Garcia, and Y. J. Su (2000), Cadmium, indium, tin, tellurium, and sulfur in oceanic basalts: Implications for chalcophile element fractionation in the Earth, *J. Geophys. Res.*, *105*(B8), 18,927–18,948, doi:10.1029/2000JB900152.

Yu, D., D. Fontignie, and J.-G. Schilling (1997), Mantle plume-ridge interactions in the Central North Atlantic: A Nd isotope study of Mid-Atlantic Ridge basalts from 30°N to 50°N, *Earth Planet. Sci. Lett.*, *146*, 259–272, doi:10.1016/S0012-821X(96)00221-X.